Student thesis series INES nr 630

Applying LPJ-GUESS on the Arctic: A model evaluation and benchmarking study

Margot J. Knapen

2023
Department of
Physical Geography and Ecosystem Science
Lund University
Sölvegatan 12
S-223 62 Lund
Sweden

Margot J. Knapen (2023)
Applying LPJ-GUESS on the Arctic: A model evaluation and benchmarking study
Tillämpning av LPJ-GUESS i Arktis: En modellutvärdering och benchmarkingstudie
Master degree thesis, 30 credits in *Physical Geography and Ecosystem Science*
Department of Physical Geography and Ecosystem Science, Lund University

Level: Master of Science (MSc)

Course duration: *January* 2023 until *June* 2023

Applying LPJ-GUESS on the Arctic: A model evaluation and benchmarking study

---

Margot J. Knapen

Master thesis, 30 credits, in *Physical Geography and Ecosystem Science*

Supervisor:
Stefan Olin, Lund University

Exam committee:
David Wårlind, Lund University
Alexandra Pongracz, Lund University

Acknowledgements

I would like to thank my supervisor, Stefan Olin, for his help and support throughout this project. I would also like to express my gratitude to Marko Scholze for his guidance and valuable feedback. My special thanks go to the staff at INES, especially Adrian Gustafsson who has helped me with the bias correction and Alexandra Pongracz for sharing her version of LPJ-GUESS with me. Lastly, I would like to thank my parents for giving me the love, support and encouragement I needed to complete this thesis.

Abstract

Warming in the Arctic occurs at a much higher rate than the global average, which has a considerable impact on the Arctic terrestrial carbon cycle. Permafrost thawing can release substantial amounts of carbon, whilst tundra shrubification and tree-line advance, on the other hand, may compensate for this. To gain a better understanding of the Arctic carbon cycle in the future, global dynamic vegetation models (DGVMs) can be used to simulate vegetation properties and dynamics.

The aim of this study was to evaluate the performance of LPJ-GUESS, a DGVM, when it is applied on the Arctic to gain a better understanding how well the model is able to capture certain key Arctic-related processes and variables. The study focussed primarily on gross primary productivity (GPP), ecosystem respiration (R_{eco}), active layer thickness (ALT) and snow depth. A total of 20 (sub-)Arctic FLUXNET sites were included. The model was forced with a bias-corrected climate forcing based on meteorological observations for each site. Different simulations were evaluated, including an upland, wetland and wet forest run.

This study has shown that LPJ-GUESS tends to underestimate GPP and R_{eco}, especially for high Arctic sites (>70°N). ALT at the end of the season (August/September) is largely overestimated for the upland simulation, whereas it is underestimated for wetlands. Running the model as a wet forest (i.e. wetland with tree PFTs) resulted in a very good fit for ALT. However, it also led to a large decrease in the modelled GPP and R_{eco}. Snow depth was poorly captured by the model, with large underestimations at most sites.

In light of these insights, it is evident that refining the LPJ-GUESS model remains essential for comprehending the intricate dynamics of the Arctic carbon cycle. Furthermore, this study accentuates the capacity and promise associated with the utilization of DGVMs in emulating vegetation attributes and behaviours.

Keywords: Physical Geography and Ecosystem Analysis; LPJ-GUESS; Arctic; FLUXNET; Gross Primary Productivity; Ecosystem Respiration; Permafrost; Active Layer Thickness; Snow Depth

Contents

List of abbreviations

Abbreviation	Meaning	Unit
ABCflux Dataset	Arctic-Boreal CO_2 Fluxes Dataset	
AGB	Above Ground Biomass	kgC m^{-2}
ALT	Active Layer Thickness	cm
BC	Bias Corrected	
CALM	Circumpolar Active Layer Monitoring	
CH_4	Methane	
CO_2	Carbon Dioxide	
CRU	Climatic Research Unit	
CUT	Constant USTAR Threshold	
DGVM	Dynamic Global Vegetation Model	
fPAR	Fraction of PAR absorbed by foliage	
GDD	Growing Degree Day	
GPP	Gross Primary Productivity	gC m^{-2} d^{-1}
ISIMIP	Inter-Sectoral Impact Model Intercomparison Project	
JULES	Joint UK Land Environment Simulator	
JRA	Japanese Reanalysis	
LAI	Leaf Area Index	m^2 m^{-2}
LPJ-GUESS	Lund-Potsdam-Jena General Ecosystem Simulator	
LSM	Land Surface Model	
N	Nitrogen	
NCEP	National Centers for Environmental Prediction	
NEE	Net Ecosystem Exchange	gC m^{-2} d^{-1}
P	Phosphorus	
PAR	Photosynthetically-Active Radiation	J m^{-2} d^{-1}
PFT	Plant Functional Type	
R^2	Coefficient of Determination	
R_a	Autotrophic Respiration	gC m^{-2} d^{-1}
R_h	Heterotrophic Respiration	gC m^{-2} d^{-1}
R_{eco}	Ecosystem Respiration	gC m^{-2} d^{-1}
RMSE	Root Mean Square Error	
SLA	Specific Leaf Area	m^2 kg^{-1}
VUT	Variable USTAR Threshold	

1 Introduction

Climate change has a considerable impact on the Arctic, where warming occurs two to three times as fast as the global average (Chylek et al. 2022). The largest change in air temperature can be observed in the cold season (Box et al. 2019). Generally speaking, the Arctic is experiencing an increase in low-level clouds, humidity and precipitation. The latter is problematic as, due to the rising temperatures, there might be relatively more rain than snow (Box et al. 2019).

Large areas of the Arctic and sub-Arctic are underlain by permafrost, which is defined as ground that stays frozen for two consecutive years or more (Harris et al. 1988). It is estimated that permafrost soils contain one third of the carbon stored in the global near-surface soil carbon pool (0-3 meters depth), whilst only extending across 15% of this pool's area globally (Schuur et al. 2015; Meredith et al. 2019).

Increasing near-surface air temperature and changes in snow regimes is causing permafrost degradation, which releases substantial amounts of greenhouse gases such as carbon dioxide (CO_2) and methane (CH_4) (Biskaborn et al. 2019; Bruhwiler et al. 2021). These CO_2 and CH_4 emissions can in turn further enhance climate change (Schuur et al. 2008), which could indicate that the Arctic would shift from being a carbon sink to a carbon source. Certain compensating processes which take up carbon, such as tree-line advance and shrubification, are expected to intensify (Zhang et al. 2013; Martin et al. 2017). On the other hand, increased shrub coverage lowers the albedo which will lead to further warming (Miller and Smith 2012).

To better understand how the Arctic terrestrial carbon cycle may change in the future, and how it will influence climate change, it is of great importance that these processes can be accurately simulated by climate and vegetation models (Chadburn et al. 2017). This study uses the Lund-Potsdam-Jena General Ecosystem Simulator (LPJ-GUESS), which is a dynamic global vegetation model (DGVM) (Smith et al. 2014). LPJ-GUESS can simulate vegetation dynamics based on the climate forcing and the soil characteristics as input data. Since version 4.1, the model has become more suitable for studies in the Arctic as some key Arctic-related components have been introduced, such as permafrost dynamics and Arctic plant functional types (PFTs). Some recent studies have made use of these new features, such as Gustafson et al. (2021) who looked at tree-line advance and Pongracz et al. (2021) who proposed a new dynamic snow scheme. Nevertheless, there is still a need for additional studies that evaluate how well LPJ-GUESS performs when applied on Arctic sites.

1.1 Aim of study

The aim of this study is to assess the ability of LPJ-GUESS to simulate important Arctic processes that can improve our understanding of the ecosystem's response to the changing climate. More specifically, it focusses on vegetation carbon fluxes (gross primary productivity (GPP) and ecosystem respiration

(R_{eco})), active layer thickness (ALT) and snow depth. The current state of the model is evaluated. LPJ-GUESS output, from a run with default parameter values, is compared to observations for FLUXNET sites located in the Arctic. Since many Arctic sites are wetlands, LPJ-GUESS is also run with wetland PFTs and peat soils. To improve the model's performance for wet forests, an additional simulation is included where tree PFTs are allowed to grow on wetlands. Two other variables, leaf area index and biomass, are studied to better understand the model's behavior.

2 Theoretical background

2.1 Arctic vegetation

The Arctic can be roughly divided into three zones based on their treeline latitudinal bound (Eugster et al. 2000). Tundra can be found north of the treeline, and is covered by low-growing vegetation such as grasses, mosses and shrubs (Walker et al. 2005). The boreal zone can be found south of the treeline, until roughly 50ºN. This region is dominated by evergreen coniferous trees, although deciduous conifers (e.g. larch) and broadleaved trees are widespread as well (Kasurinen et al. 2014). The subarctic zone is located in proximity to the treeline and is characterized by open forests where tree growth is highly limited by the short growing season (Eugster et al. 2000).

Climate change is affecting the vegetation in the Arctic in various ways (Mod and Luoto 2016). Different climatic conditions can alter the species distributions (Elmendorf et al. 2012). Furthermore, an increase in woody vegetation is being observed, a process which is commonly referred to as shrubification (Epstein et al. 2012; Myers-Smith and Hik 2018). This may enhance competition and consequently affect biodiversity (Wookey et al. 2009). Shrubficiation, mainly in terms of increased biomass and cover, can influence the productivity of an ecosystem (Martin et al. 2017). Yet, warming is also likely to intensify soil respiration which would counteract the increase in productivity to a certain extent (Bruhwiler et al. 2021).

2.1.1 Wetlands

Approximately 25% of the total of the Arctic's land area can be classified as wetland (Kåresdotter et al. 2021). The type of vegetation in these high latitude wetlands is largely dependent on its acidity and soil moisture. GPP in these ecosystems is mainly affected by the availability of, or often times lack of, nitrogen (N) and phosphorus (P). This implies that (rain-fed) bogs are generally less productive than fens, where nutrients are supplied through ground or surface water (Jonasson and Shaver 1999).

2.2 Carbon fluxes in the Arctic

Vegetation carbon fluxes are important indicators of the response of Arctic ecosystems to the changing climate (Kira et al. 2021; Ma et al. 2021). GPP is defined as the rate of carbon fixation by primary producers through photosynthesis (Reichle 2020). R_{eco} consists of all respiration within an ecosystem and can thus be defined as $R_{eco} = R_a + R_h$, where R_a and R_h are autotrophic and heterotrophic respiration, respectively. The sum of GPP and R_{eco} is the net ecosystem exchange (NEE).

NEE can be measured by eddy-covariance systems and can be partitioned into GPP and R_{eco}. This can be done by fitting a function of temperature to nighttime R_{eco} which can then be used to calculate daytime R_{eco} and thus also GPP (Reichstein et al. 2005). Another approach makes use of the light-response curves where daytime NEE is fitted to, and from which respiration can be approximated (Lasslop et al. 2010).

In the Arctic, GPP tends to reach its maximum in July, whilst being close to zero during the November to March winter months (Ma et al. 2021). Rising temperatures and the lengthening of the growing season are both factors that are likely to lead to enhanced GPP (Bruhwiler et al. 2021). The increased soil temperatures can, on the other hand, counteract this carbon uptake by enhancing respiration (Piao et al. 2008).

The leaf area index (LAI) and GPP are closely related to each other, especially during the first half of the season. This means that if a model can accurately simulate LAI, it will generally also perform well for GPP. When the incoming solar radiation declines during the second half of the season, a reduction in GPP can be observed.

R_{eco} consists of two components: plant respiration and heterotrophic respiration. Plant respiration behaves in a similar fashion to GPP being highly sensitive to temperature, LAI and incoming solar radiation (Chadburn et al. 2017). Heterotrophic respiration, on the other hand, is dependent on the conditions below-ground. As a consequence, it is mainly driven by air temperature and, more importantly, the soil temperature. This is also the reason why GPP and R_{eco} show a very different seasonal cycle (Chadburn et al. 2017).

Both GPP and R_{eco} are dependent on soil moisture (Chadburn et al. 2017). In the Arctic, soil moisture is to some extent governed by the amount, and change in, snowfall. This can affect the wetness of the soil during summer and consequently affect vegetation carbon fluxes.

2.3 Permafrost

Permafrost, commonly defined as ground, at any depth, that remains frozen for two consecutive years or more, is widespread in the (sub-)Arctic. It is estimated that permafrost soils cover roughly 25% of the land surface in the Northern Hemisphere (Gruber 2012). As a result of the rapid climate change in

the Arctic, soil temperatures increase which stimulates permafrost degradation (Schaefer et al. 2014). Large quantities of carbon that were stored at temperatures too low for degradation to occur, are now at a risk of being decomposed into the greenhouse gases CO_2 and CH_4. This will in turn further enhance global warming and is consequently often called the permafrost carbon feedback (Schuur et al. 2015).

In addition to permafrost extent, it is of great interest to look at the active layer thickness (ALT). The active layer is often defined as the layer closest to the surface that thaws during summer and freezes during the winter months (Burn 1998). The depth to which the active layer extents is important for vegetation as it constrains the rooting zone (Blume-Werry et al. 2019). ALT is dependent on various factors such as the insulating effect of overlying snow, types of vegetation, air temperature and the wetness of the soil (Luo et al. 2016).

2.4 Snow

Snowfall and the presence of a snow pack have a large impact on Arctic ecosystems. The melting of snow provides large quantities of melt water, consequently affecting the hydrology. In the Arctic, snow insulates the ground and as a consequence more energy is needed to cause the melting of the snow pack. This is different as opposed to temperate regions, where melt is stimulated by the minor heat fluxes from the ground (Eugster et al. 2000).

The drivers behind snow accumulation are not fully understood, but both the canopy and heterogeneity in the topography play an important role (Eugster et al. 2000). How snow is distributed in the landscape is mainly governed by wind. At open tundra sites, the snow cover distribution can vary a lot whereas snow is usually more evenly distributed at forest sites.

As a result of climate change, a decline in the area covered by snow, the number of snow days and the depth of snow packs is being observed (Box et al. 2019).

2.5 LPJ-GUESS

The DGVM used in this study is the Lund-Potsdam-Jena General Ecosystem Simulator (LPJ-GUESS) (Smith et al. 2014). Based on climate forcing and soil input data, the model simulates vegetation dynamics and biogeochemical processes at a given land grid cell. As a result of light competition, the availability of nutrients and the presence of soil water, different types of vegetation will emerge and grow. Each plant individual belongs to a certain plant functional type (PFT), which describes common parameters for e.g. bioclimatic limits, phenology and shade (in)tolerance. Since version 4.1, some key Arctic-related components, e.g. permafrost dynamics and Arctic PFTs, are incorporated in the model, which are explained in more detail in the sections below.

2.5.1 Soil temperature and active layer thickness

Since LPJ-GUESS version 4.1, the approach to calculate the soil temperatures has been improved. This is important when applying the model on the Arctic as ALT simulated by LPJ-GUESS is dependent on soil temperature. The active soil column is composed of 15 layers which each are 10 cm thick. This implies that the maximum ALT simulated by LPJ-GUESS is 150 cm. The surface layer can be overlain by snow, which has an insulating effect (see *2.5.2 Dynamic snow scheme*). Below the active soil column, 5 padding layers extend to a depth of 48 m.

On a daily basis, the thermal diffusivity of each soil layer is calculated based on its heat capacity and thermal conductivity. Upland soils are made up of a certain percentage of mineral components, organic components and pore spaces, the latter which are filled by ice, water and air. The thermal conductivity and heat capacity differ for each of these components. The temperature of the surface layer is influenced by the air temperature. ALT is updated daily with the depth of the soil layers where the soil temperature is higher than 0 ^{o}C.

2.5.1.1 Peat soils

The soil column of wetlands differs from upland sites, which influences ALT. Similar to upland soils, peatlands consist of 15 active soil layers and 5 padding layers. The 3 uppermost layers are part of the acrotelm with a varying water table, whereas the other 12 layers comprise the permanently saturated catotelm. The calculation of the soil temperature is done in a similar fashion as described in *2.5.1 Soil temperature and active layer depth*. However, at wetland sites the soil is composed of fixed fractions of peat, rather than mineral and organic soil components and thus different values for the thermal conductivity and heat capacity is used to derive soil temperatures.

2.5.2 Dynamic snow scheme

Up until LPJ-GUESS version 4.0, a static snow scheme was implemented which only considered one single layer. Thermodynamic properties were calculated based on a set of constants. However, Pongracz et al. (2021) have shown that this snow scheme does not fully capture cold season processes. Since version 4.1 the simple multi-layer snow scheme developed by Pongracz (2019) has been incorporated in the model. Since then Pongracz et al. (2021) have been working on a more advanced, dynamic snow scheme. A short description of the dynamic snow scheme, which was used in this study, is given below.

The daily amount of snowfall is dependent on the air temperature and precipitation as climate forcing. The dynamic snow scheme also requires input on wind speed as this is used to calculate the fresh snow density. There can be a maximum of five layers of snow, where a new layer of snow is initialized if a certain threshold has been exceeded. For the first layer the threshold lies at 100 mm, after which the threshold increases by 50 mm per layer. Fresh snow is added to the top layer. However, if the snow depth reaches 250 mm, snow accumulates at the bottom snow layer. Snow density and the ice content

of a layer are used to calculate the depth of each layer. The density can change either due to mechanical compaction or phase changes.

Snow melt is dependent on the internal temperature of each layer. The thermal properties (thermal conductivity, heat capacity, diffusivity) differ from layer to layer. The thermal conductivity is dependent on the layer's density, whereas both the density and temperature are required to calculate the heat capacity. The diffusivity of a layer is given by dividing its thermal conductivity by its heat capacity. These thermal properties are then used to calculate the new internal temperature of each snow layer, which is used for determining snow melt. Meltwater is allowed to percolate into the soil, if it is not frozen.

2.5.3 Plant functional types

Vegetation simulated by LPJ-GUESS is grouped in so-called plant functional types (PFTs) based on similar characteristics and traits. The model provides a list of pre-defined and parameterized Arctic- and wetland-specific PFTs, see *Table 1*.

Table 1. Arctic and wetland PFTs included in LPJ-GUESS version 4.1.

Arctic PFT	Wetland PFT	Description
BNE		Boreal needleleaved evergreen tree, shade-tolerant
BINE		Boreal needleleaved evergreen tree, shade-intolerant
BNS		Boreal needleleaved summergreen tree, shade-intolerant
IBS		Shade-intolerant broadleaved summergreen tree
C3G		C3 grass
HSE		Evergreen tall shrub
HSS		Summergreen tall shrub
LSE	pLSE	Evergreen low shrub
LSS	pLSS	Summergreen low shrub
GRT		Graminoid and forb tundra
EPDS		Evergreen prostrate dwarf shrub
SPDS		Summergreen prostrate dwarf shrub
CLM	pCLM	Cushion forb, lichen and moss tundra
	pmoss	Moss
	wetGRS	Flood-tolerant C3 grass

2.5.4 Vegetation carbon fluxes in LPJ-GUESS

LPJ-GUESS calculates the GPP using a simplified version of the Farquhar and von Caemmerer (1982) photosynthesis model. This calculation involves several inputs such as atmospheric CO_2 concentration, average air temperature, cumulative daily photosynthetically-active radiation (PAR), and the proportion of PAR absorbed by foliage (fPAR).

A crucial element in these calculations is V_{max}, which signifies the upper limit of the Rubisco enzyme's carboxylation rate. When daily conditions are not constrained by water stress, LPJ-GUESS determines V_{max} for each day, considering factors like air temperature, PAR, and the availability of nitrogen.

R_{eco} comprises two components: soil respiration and autotrophic respiration. Soil respiration is determined by the dynamics of soil organic matter (SOM) and the release of carbon into the atmosphere through decomposition processes. Autotrophic respiration corresponds to the daily energy needed for a plant's maintenance and growth respiration. It's important to note that leaf respiration is not included in this context, as it is subtracted from net assimilation as a fraction of V_{max}.

3 Methods

3.1 General overview

Figure 1 shows an overview of the methodology applied in this study. First, LPJ-GUESS was run using global gridded CRUJRA data (University of East Anglia Climatic Research Unit and Harris 2020). Using FLUXNET observations on meteorological variables, the CRUJRA data was bias corrected (BC). Next, the model was run with the bias corrected climate forcing. This was repeated three times: (1) no wetland PFTs were included ("upland"), (2) wetland PFTs were included and the landcover class was set to peatland ("wetlands") and (3) same as (2) but with BNE and BINE trees ("wetlands with trees").

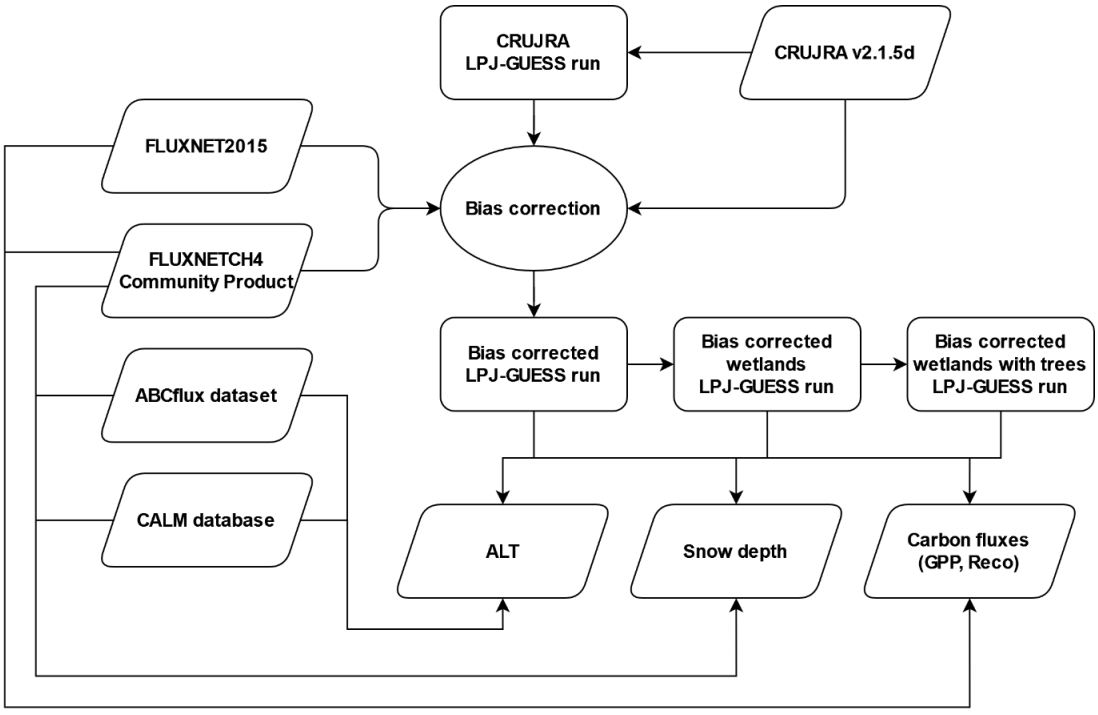

Figure 1. Schematic overview of the data used in this study, the different LPJ-GUESS simulations that were run and the output variables that were evaluated.

3.2 Evaluation data

The model's performance was evaluated using observational datasets. This study relied mainly on data from the FLUXNET2015 dataset (Pastorello et al. 2020) and the FLUXNETCH4 Community Product (Delwiche et al. 2021) for daily GPP, R_{eco}, NEE and climate data. The FLUXNETCH4 Community Product also contained data on snow depth. The ABCflux dataset (Virkkala et al. 2021; Virkkala et al. 2022) provided additional data on the vegetation type, ALT, snow depth, biomass and LAI. For a number of sites ALT observations were acquired from the CALM database (Brown et al. 2000).

3.2.1 FLUXNET2015

The most recent FLUXNET dataset is currently FLUXNET2015. It comprises data on, amongst other things, carbon and water fluxes, meteorological variables and energy exchange. A total of 212 sites are covered, of which seven were included in this study (see *Table B1*). The FLUXNET2015 dataset aims to apply a consistent processing and quality control methodology. Consequently, different sites can be easily compared to each other and the data tends to be of a high quality.

FLUXNET2015 includes various variables for the carbon fluxes. For this study the variables GPP_NT_VUT_REF and RECO_NT_VUT_REF were used. VUT stands for the Variable USTAR (u*) Threshold which means that a variable threshold was used for friction velocity. The quality of NEE data obtained by eddy covariance techniques depends to a certain extent on the level of turbulence, where NEE tends to be underestimated if there is little turbulence. VUT, as opposed to the Constant USTAR Threshold (CUT), is commonly used when there is a clear seasonality in carbon fluxes at the site of interest. NT stands for the Night-Time partition method and refers to the methodology that has been applied by FLUXNET when GPP and R_{eco} were derived from the observed NEE (Wutzler et al. 2018).

The FLUXNET2015 dataset includes information about the quality of the data. A similar approach for data cleaning was applied as described in Ma et al. (2021), where GPP and R_{eco} data points (below denoted by "X") were set to NA if any of the following three conditions were met:

1. The value for NEE_VUT_REF_NIGHT_QC (i.e. the corresponding quality flag) was lower than 0.5.
2. There was a difference of more than 50% between X_DT_VUT_REF and X_NT_VUT_REF.
3. The value for X_NT_VUT_REF was negative.

The FLUXNET2015 dataset does not provide data on relative humidity, but this was instead derived from the vapour pressure deficit as described in Jones (2013) (see *Appendix A*).

3.2.2 FLUXNETCH4 Community Product

The FLUXNETCH4 Community Product Version 1.0 was published in 2021 and is an open-source dataset containing data from 79 sites, 13 of which are located in the study area (see *Table B2*). For the

meteorological data and NEE, the gap-filled variables were used. For GPP and R_{eco}, the night-time partition method was used. No additional quality control was performed, although a few sites contained some clearly incorrect values (e.g. GPP exceeding 10^{20} µmol CO_2 m^{-2} s^{-1}) which were removed. The carbon fluxes were converted from µmol CO_2 m^{-2} s^{-1} to gC m^{-2} d^{-1}.

For five sites, the dataset also included daily snow depth observations, which were aggregated to monthly mean values.

3.2.3 ABCflux database

The ABCflux (Arctic-boreal CO_2 flux) database provides monthly data for 244 sites in the Arctic-boreal zone on meteorological variables and carbon fluxes. Most of the sites in this study were represented in the ABCflux database with ancillary data on variables such as ALT, snow depth, vegetation types, LAI, above ground biomass (AGB) and soil properties.

For AGB, the ABCflux database specified for each site which types of above ground vegetation were included in the measurement. At some sites, such as US-Prr, only trees were taken in consideration whereas at other sites (e.g. US-Uaf) mosses were included as well.

The LPJ-GUESS output for biomass only provides the sum of above and belowground biomass, rather than the individual components. To be able to compare the observations to the simulated, the total biomass was approximated from the observed AGB. This was done based on the findings from a paper by Noguchi et al. (2012). They found that for their black spruce forest site in interior Alaska, 47% of the biomass in the vascular plants was stored belowground. When also accounting for AGB by mosses, 53% of the biomass is stored aboveground.

3.2.4 CALM database

The CALM database was set up in the early 1990s and provides data on ALT for more than 100 sites. This makes it possible to study the long-term response of ALT to the changing climate. Measurements are gathered using set protocols and usually between 20- and 120-point measurements are taken within a regular grid of 10x10 m to 1000x1000 m. Data from six of the CALM sites was used as they were at roughly the same location as the FLUXNET sites.

3.2.5 Study area

All FLUXNET sites at a latitude of at least 64°N that were available following the CC-BY-4.0 usage license were included (see *Figure 2*, *Table B1*, *Table B2*). The CALM sites with ALT data that were used, and their corresponding FLUXNET site, are listed in *Table B3*.

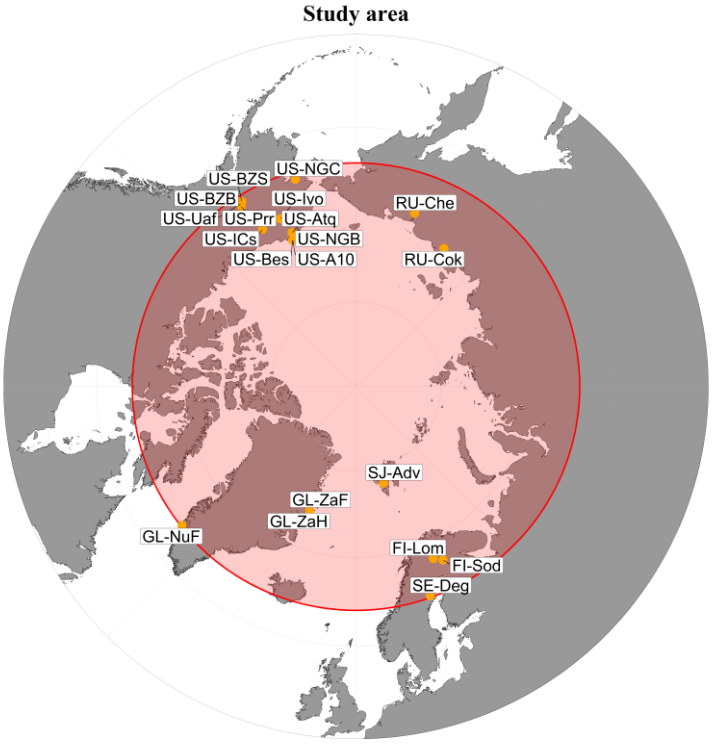

Figure 2. Map showing the 20 FLUXNET sites located above 64°N (red area).

3.3 Model set-up & forcing data

In this study, a version of LPJ-GUESS 4.1 was used which included the dynamic snow scheme that has recently been developed by Pongracz et al. (2021). Some changes to the source code were made to ensure that daily output for GPP and R_{eco} was supported.

LPJ-GUESS was run in cohort mode with a spin-up phase of 500 years and 50 replicate patches. The fire module was switched off. CO_2 data was taken from Tans (2023). CRUJRA v2.1.5d was used as climate forcing which contains 6-hourly data for mean air temperature, precipitation, wind speed, incoming solar radiation and specific humidity. LPJ-GUESS required a climate forcing on a daily timestep, rather than a 6-hourly. For this reason, the 6-hourly data was aggregated to daily means or, in the case of precipitation, to the daily sum.

Initially the latest version of CRUJRA (v2.3.5d) was used (University of East Anglia Climatic Research Unit and Harris 2022), but it became apparent that there were large differences in shortwave radiation when comparing it to both CRUNCEP (Viovy 2018) and CRUJRA v2.1.5d data.

Table 2 shows the meteorological variables and their units that were required by LPJ-GUESS and that were available in the CRUJRA and FLUXNET data. Zonal and meridional wind speeds were used to derive the directionless wind speed. Relative humidity was calculated from specific humidity, see *Appendix A*.

Table 2. Meteorological variables and their units as supported by LPJ-GUESS and provided by CRUJRA and FLUXNET.

	LPJ-GUESS		CRUJRA		FLUXNET	
Variable	**Name**	**Unit**	**Name**	**Unit**	**Name**	**Unit**
Mean temperature	temp	K	tmp	K	TA	degC
Precipitation	prec	mm d^{-1}	pre	mm $6h^{-1}$	P	mm d^{-1}
Incoming solar radiation	insol	W m^{-2}	dswrf	J m^{-2} $6h^{-1}$	SW_IN	W m^{-2}
Wind speed	wind	m s^{-1}	vgrd, ugrd	m s^{-1}	WS	m s^{-1}
Pressure	pres	Pa	pres	Pa	PA	kPa
Specific humidity	specifichum	kg kg^{-1}	spfh	kg kg^{-1}		
Relative humidity	relhum				RH	%
Vapour pressure deficit					VPD	hPa

3.4 Bias correction

The CRUJRA data was bias corrected on a monthly basis using the ISIMIP3BASD v1.0 method (Lange 2022). This approach is based on parametric quantile mapping and ensures that trends are preserved. This variant of quantile mapping entails fitting a probability distribution, such as the normal or gamma distribution, to the data prior to mapping the quantiles (Lange 2019). The aim was to align the distribution of the FLUXNET and CRUJRA data such that biases in both the mean and variance of each variable in the CRUJRA data were reduced.

There are various settings that can be modified so that the bias adjustment approach fits the variable. For this study similar specifications were used as in Lange (2019), see *Table 3*. Temperature was the only variable that was detrended. Upper bound scaling was applied on shortwave radiation. This implies that the data was initially constrained to an interval of [0, 1] and scaled back to values within the actual range after the bias correction.

If there were no observations for a certain variable available, CRUJRA data was used instead. This was necessary for shortwave radiation for US-Atq and US-NGC. The FLUXNET observations for precipitation at FI-Lom were unlikely high and were as a consequence also replaced by CRUJRA data.

After the bias correction was completed, the observations were copied back into the file. In this way, the bias corrected climate forcing was only used for those years where no observations were available.

Table 3. Parameter settings for the bias correction as described in Lange (2022).

Variable	**Lower bound**	**Lower threshold**	**Upper bound**	**Upper threshold**	**Distribution**	**Trend preservation**	**Detrending**	**Half-window**
temp	-	-	-	-	Normal	Additive	Yes	-
prec	0	0.1/86400	-	-	Gamma	Mixed	No	-
insol	0	0.0001	1	0.9999	Beta	Bounded	No	15
wind	0	0.01	-	-	Weibull	Mixed	No	-
relhum	0	0.0001	1	0.9999	Beta	Bounded	No	-

3.5 Trees on wetlands

The boreal US-Uaf, "University of Alaska, Fairbanks", site is part of the Ameriflux network. Evergreen needleleaved trees, primarily black spruce (*Picea mariana*), grow in this bog and cover more than 60% of the land area (see *Figure 3*). It is a relatively sparse forest with around 4500 trees per hectare (Ueyama et al. 2014).

To improve the model fit for ALT, LPJ-GUESS was run with wetland PFTs and peat soils enabled. However, for sites such as US-Uaf this implied that no trees were simulated which consequently affected the GPP. For this reason, LPJ-GUESS was also run with the wetland scenario but including BNE and BINE as tree PFTs. To allow for these trees to grow in wet conditions, parameters related to the withstanding of inundation were added and the corresponding land cover class was set to peatland. By default, daily GPP is reduced in case of inundation, but this setting was disabled.

Figure 3. Photograph of the US-Uaf site taken by Ueyama (2018).

3.6 Analysis

A statistical metric that was used in the analysis of the results of this study was the root mean square error (RMSE) (Chicco et al. 2021). The RMSE for a sample of n observations Y and their corresponding model predictions X is defined as in equation (1) below. The RMSE has the same units as y and its values range between 0 and $+\infty$, where 0 indicates the best value.

$$RMSE = \sqrt{\frac{1}{n}\sum_{i=1}^{n}(X_i - Y_i)^2} \qquad (1)$$

Another metric used in this study was the coefficient of determination, or R^2. The unitless R^2 is defined as in equation (2) below. Values close to 1 are considered to indicate a better goodness-of-fit.

$$R^2 = 1 - \frac{\sum_{i=1}^{n}(X_i - Y_i)^2}{\sum_{i=1}^{n}(\bar{Y} - Y_i)^2} \quad (2)$$

4 Results

4.1 The effect of the bias correction on GDD5

The bias correction altered the number of growing degree days (GDD), see *Figure 4*. The vertical lines indicate the thresholds for the establishment of the different shrub and tree PFTs.

The GDD5 at six high Arctic sites (US-NGB, US-Bes, GL-ZaH, GL-ZaF, SJ-Adv) was too low for shrubs to establish. For another high Arctic site, US-A10, the bias correction resulted in a distinct increase in GDD5, where the mean changed from 54 to 287. This implied that both low and tall shrubs were able to establish when forcing the model with the bias corrected data.

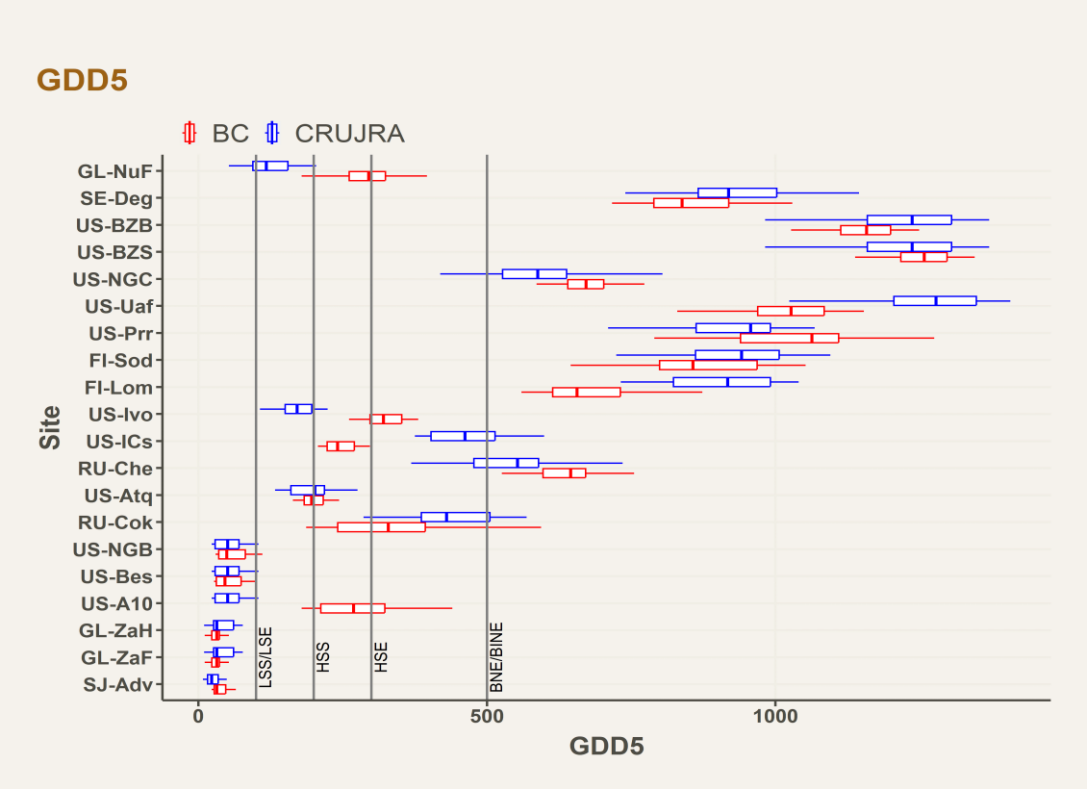

Figure 4. GDD5 for the years 1990-2010 for each site obtained from CRUJRA data (blue boxes) and the bias corrected (BC) data (red boxes). Box plots show the median, 25th percentile and 75th percentile. The whiskers indicate the minimum and maximum. The vertical lines represent the lowest GDD5 required for the PFT to establish.

4.2 Gross primary productivity

The RMSE for GPP was lower for almost all sites when running the model with the bias corrected climate forcing instead of using the CRUJRA data (see *Table C1* in *Appendix C*). The only exception being RU-Cok where the RMSE increased from 2.25 to 3.59 gC m^{-2} d^{-1}. For most wetland sites,

simulating wetland PFTs on peat soils resulted in a lower RMSE. The modelled GPP for US-BZB and US-Prr had the lowest RMSE when including tree PFTs (BNE and BINE) in the wetland simulations. This was especially true for US-Prr where the RMSE decreased from 3.37 to 1.01 gC m^{-2} d^{-1}.

LPJ-GUESS simulated values of GPP close to 0 gC m^{-2} d^{-1} for the majority of above 70°N latitude sites. Some of these sites, such as SJ-Adv and US-Bes had a low observed daily GPP with values that rarely exceeded 2.5 gC m^{-2} d^{-1}. Replacing the nitrogen deposition to a constant value of 2 kg m^{-2}, which is high for Arctic conditions, did not result in a distinct increase in GPP.

The observations indicate that some sites at high latitudes were very productive. US-A10 was, for example, one of the sites with the highest maximum daily GPP. The highest mean daily GPP (3.18 gC m^{-2} d^{-1}) was observed at RU-Cok, which is a site dominated by shrubs at 70.8°N.

Figure 5 shows the daily GPP, taken as a mean during a period of five days, for the four different simulations at US-Uaf. The upland run was closest to the 1:1 identity line, whereas the CRUJRA run

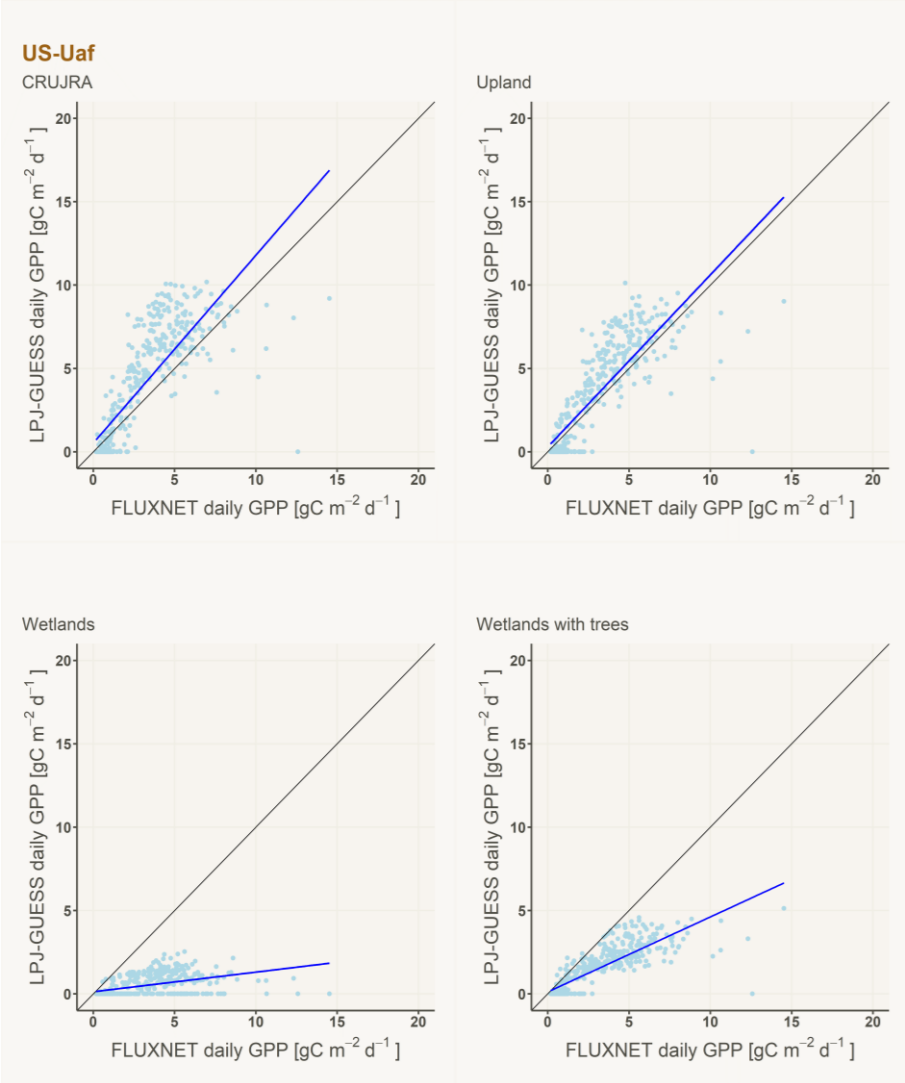

Figure 5. Daily GPP taken as a five-daily mean at US-Uaf for the four different simulations and the observations.

resulted in a slight overestimation. The wetlands run had the lowest GPP, whilst adding trees to the wetland simulation increased the GPP slightly.

Figure 6 shows the daily GPP taken as a five-daily mean for each month at US-Uaf covering all the years included in the observations (2011-2018). The upland run captured both the seasonal pattern and magnitude of GPP at this site very well. However, LPJ-GUESS failed to capture the, albeit low, GPP observed during the winter months (October-March). The simulated GPP was higher in both May and June, which indicates that the growing season started earlier than for the observations.

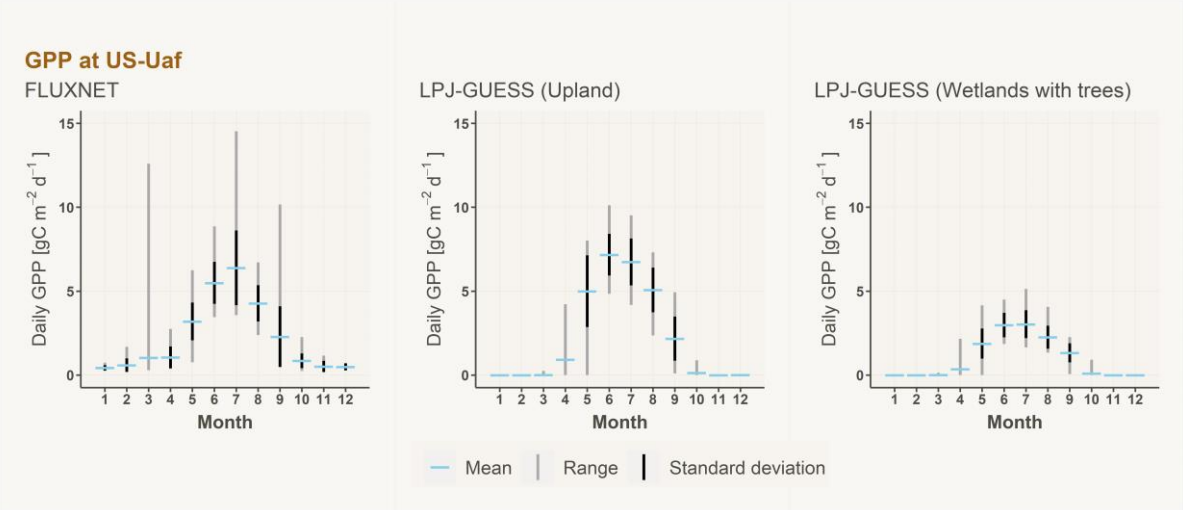

Figure 6. Daily GPP taken as a five-daily mean for the years 2011-2018 at US-Uaf. Left: FLUXNET observations. Center: LPJ-GUESS output for the bias corrected upland run. Right: LPJ-GUESS output for the bias corrected wetlands with trees run.

4.3 Biomass

While the bias-corrected upland simulation exhibited the lowest RMSE for GPP at the US-Uaf site, it failed to accurately replicate biomass patterns as evidenced by *Figure 7*. In contrast, the wetlands simulation yielded a biomass estimate that was consistent with the observed value of 0.28 kgC m^{-2}. This congruence between simulated and observed biomass was similarly observed at the US-Prr forest site.

When comparing *Figure 5* to *Figure 7*, it is evident that for the simulations a high GPP corresponds to a high biomass. However, the observations seemed to indicate an ecosystem with low biomass whilst maintaining a high productivity. This was not captured by the model.

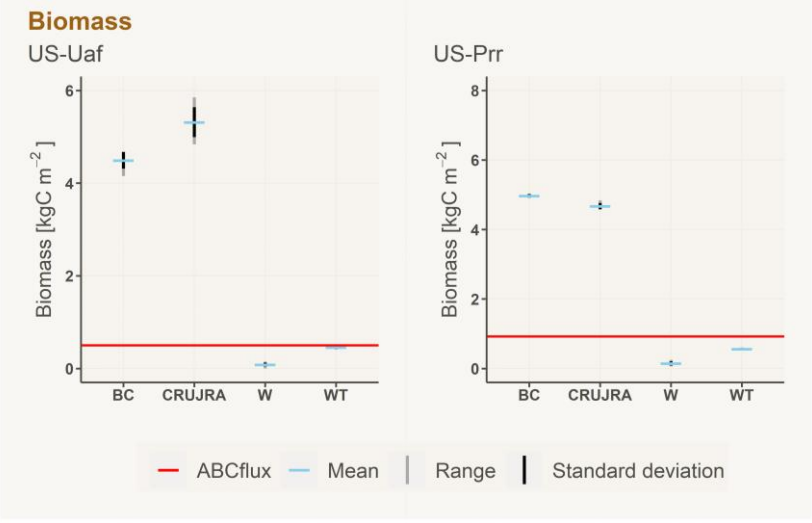

Figure 7. Biomass for US-Uaf (2003-2018) and US-Prr (2010-2016). US-Uaf includes both tree and moss PFTs, whereas US-Prr only considers the tree PFTs.

4.4 Leaf area index

LAI observations from the ABCflux dataset were available for US-Uaf. As can be seen in *Figure 8*, LPJ-GUESS overestimated the LAI, primarily during the winter months. The mean observed LAI in January was, for instance, 0.19 m^2 m^{-2} whereas LPJ-GUESS simulated 1.49 m^2 m^{-2} for this same month in the upland run. The wetlands with trees run showed a much larger range of simulated LAI, but lowered the mean LAI for the winter months which was in accordance with the observations.

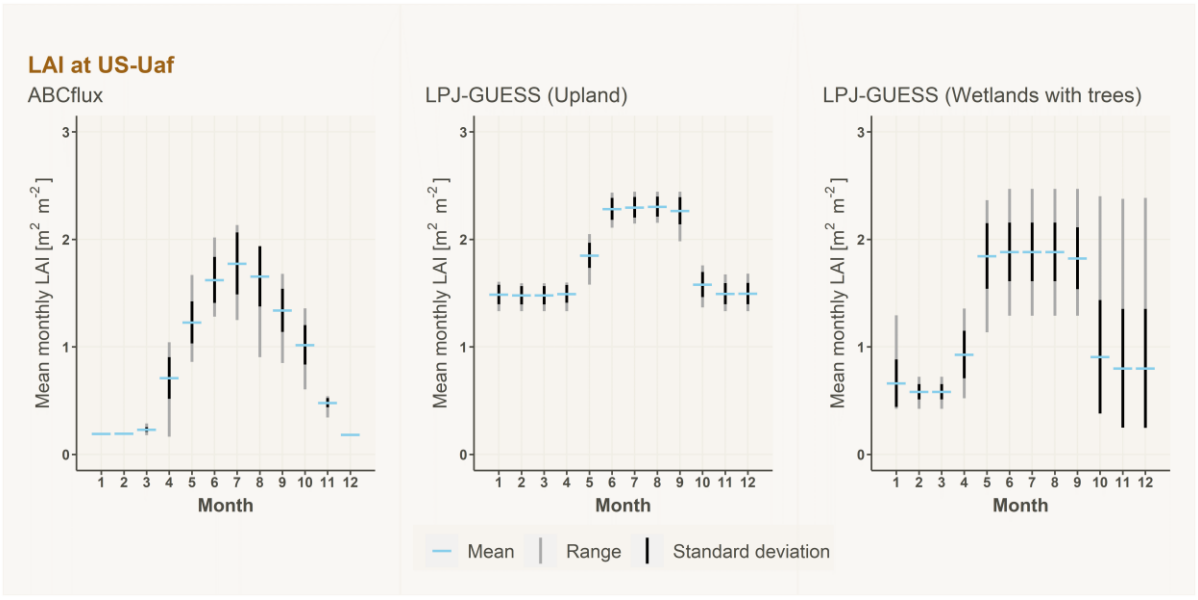

Figure 8. Mean monthly LAI for the years 2003-2018 at US-Uaf. Left: ABCflux observations. Center: LPJ-GUESS output for the bias corrected upland run. Right: LPJ-GUESS output for the bias corrected wetlands with trees run.

4.5 Ecosystem respiration

For most sites, the run with the lowest RMSE for GPP also resulted in the lowest RMSE for R_{eco} (see *Table D1* in *Appendix D*), although there were a few exceptions. At GL-NuF, for example, the model performed slightly better for R_{eco} with the BC wetland run (RMSE: 0.56 gC m^{-2} d^{-1}) than the BC upland run (RMSE: 0.58 gC m^{-2} d^{-1}). Yet, for GPP the opposite was true where the upland run had an RMSE of 1.27 gC m^{-2} d^{-1} instead of 1.39 gC m^{-2} d^{-1}.

For R_{eco} there were two sites where the model performed considerably better when using CRUJRA forcing as opposed to the bias corrected data. For RU-Cok the CRUJRA run had an RMSE of 1.08 gC m^{-2} d^{-1} whereas the bias corrected run had an RMSE of 2.01 gC m^{-2} d^{-1}. For the other Russian site, the RMSE was 0.54 gC m^{-2} d^{-1} and 0.75 gC m^{-2} d^{-1}, respectively.

One of the sites where the model seemed to capture R_{eco} very well was FI-Sod, with an RMSE of 0.80 gC m^{-2} d^{-1} and R^2 of 0.87 for the bias corrected upland simulation. *Figure 9* shows the modelled R_{eco} per month. This plot shows that the largest differences in the simulated R_{eco} occurred during May. Unfortunately, this month was poorly represented in the observations and had to be excluded.

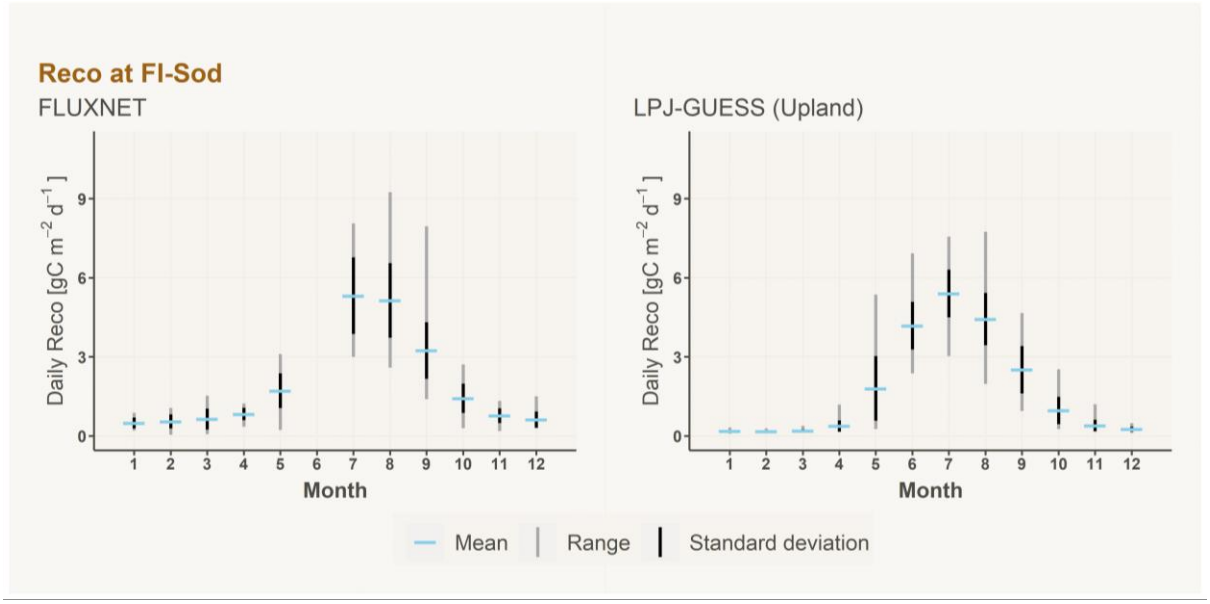

Figure 9. Daily R_{eco} taken as a five-daily mean for the years 2001-2014 at FI-Sod. Left: FLUXNET observations. Right: LPJ-GUESS output for the bias corrected upland run.

4.6 Active layer thickness

Figure 10 shows the ALT at the six CALM sites observed during the end of the season (August or September). US-A10 is classified as a site with little vegetation, whilst US-BZS is dominated by evergreen needleleaved trees. The other four sites are wetlands. From *Figure 10* it is evident that LPJ-GUESS failed to accurately simulate end-of-season ALT at wetlands. When running the model as upland sites, the ALT tended to be overestimated whereas switching on the wetland PFTs resulted in a too shallow active layer.

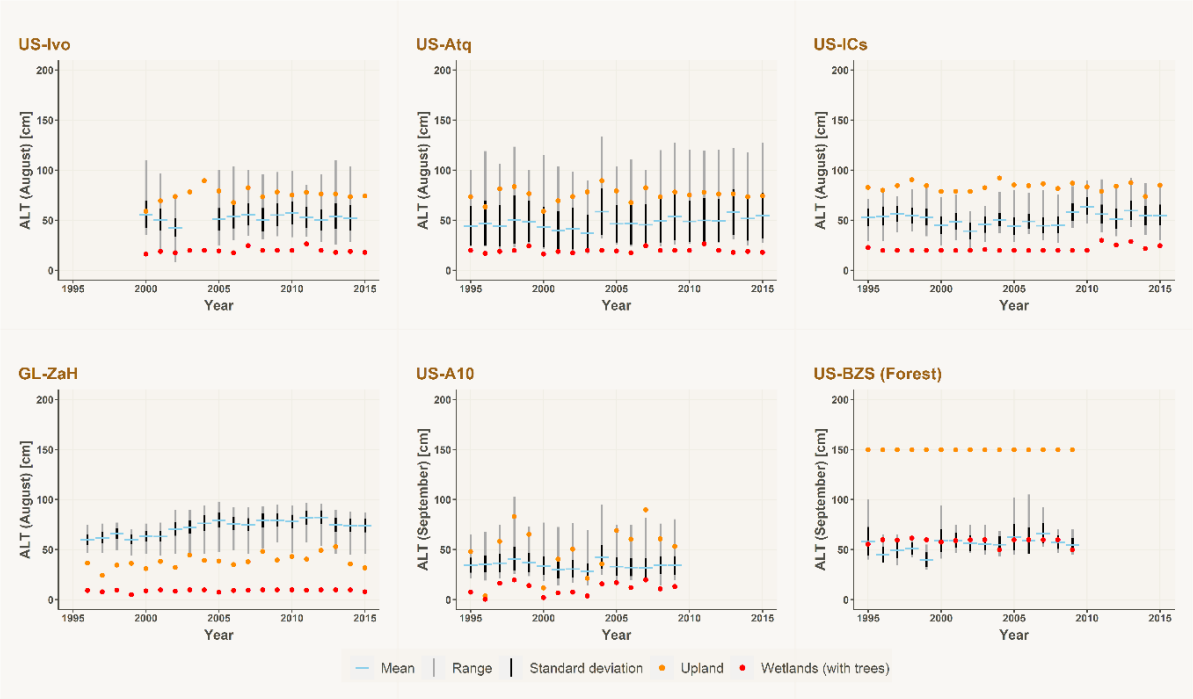

Figure 10. End-of-season (August or September) ALT. Mean, range and standard deviation are taken from the ABCflux dataset. Orange points show the LPJ-GUESS value of the bias-corrected upland simulation and the red dots represent the bias-corrected wetlands run. The exception being the forest site US-BZS, where the red dots indicate the wetlands with trees run.

For the forest site, US-BZS, the upland ALT reached the maximum of 150 cm for every year. However, when including the wetland PFTs and running the model with peat soils, the modelled ALT was in between one standard deviation of the mean for almost all years.

Data on the monthly thaw depth throughout the year was available from the ABCflux dataset for US-Uaf, see *Figure 11*. This plot illustrates the improvement in modelled ALT when assuming wetland conditions at this forest site. The RMSE dropped from 52 cm to 7 cm. It also shows observations for the soil temperature at a depth of 50 cm. The RMSE decreased from 3.72 °C to 2.00 °C. Instead of overestimating temperatures above 0 °C, LPJ-GUESS simulated values close to the freezing point for the wetlands with trees run.

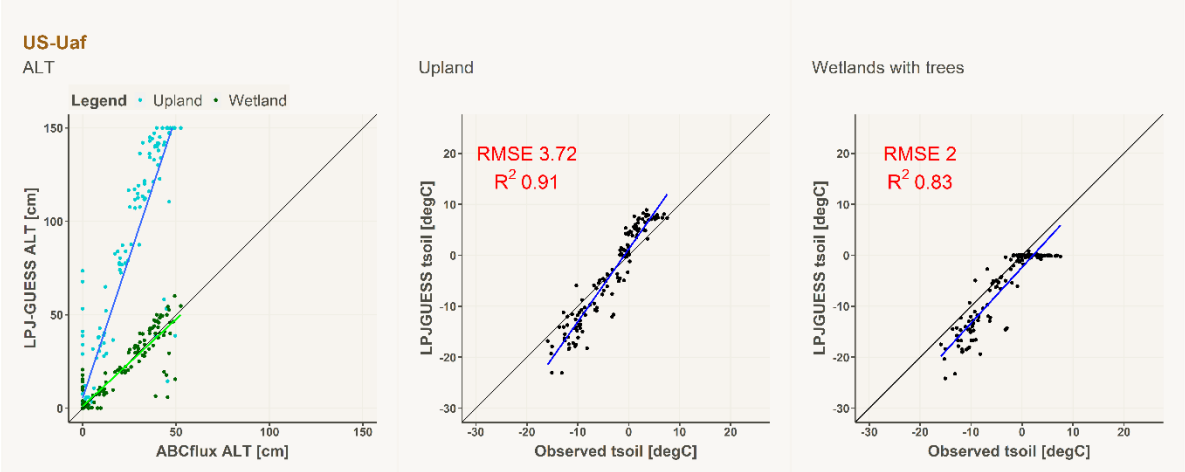

Figure 11. Simulated and observed ALT for US-Uaf (left). Simulated and observed soil temperature at 50 cm depth for the bias-corrected upland run (center) and the bias-corrected wetlands with trees run (right).

4.7 Snow depth

LPJ-GUESS simulated a too low monthly snow depth for all nine sites as shown in *Figure 12*. LPJ-GUESS performed best for US-Atq and US-Prr. The modelled snow depth was especially poorly captured for US-BZB, US-ICs and RU-Che, where all data points had a value close to 0 cm.

Figure 13 shows how the monthly snow depth differed per month for the years 2010 to 2016 at US-Uaf and US-Prr. At US-Uaf the observed snow depth greatly exceeded the simulated output during the winter months. During summer the snow depth reached 0 cm both for the observations and simulations. At US-Prr, the observed snow depth never reached 0 cm. The monthly variability was captured quite well, but the simulated snow depth was distinctly lower than the observations.

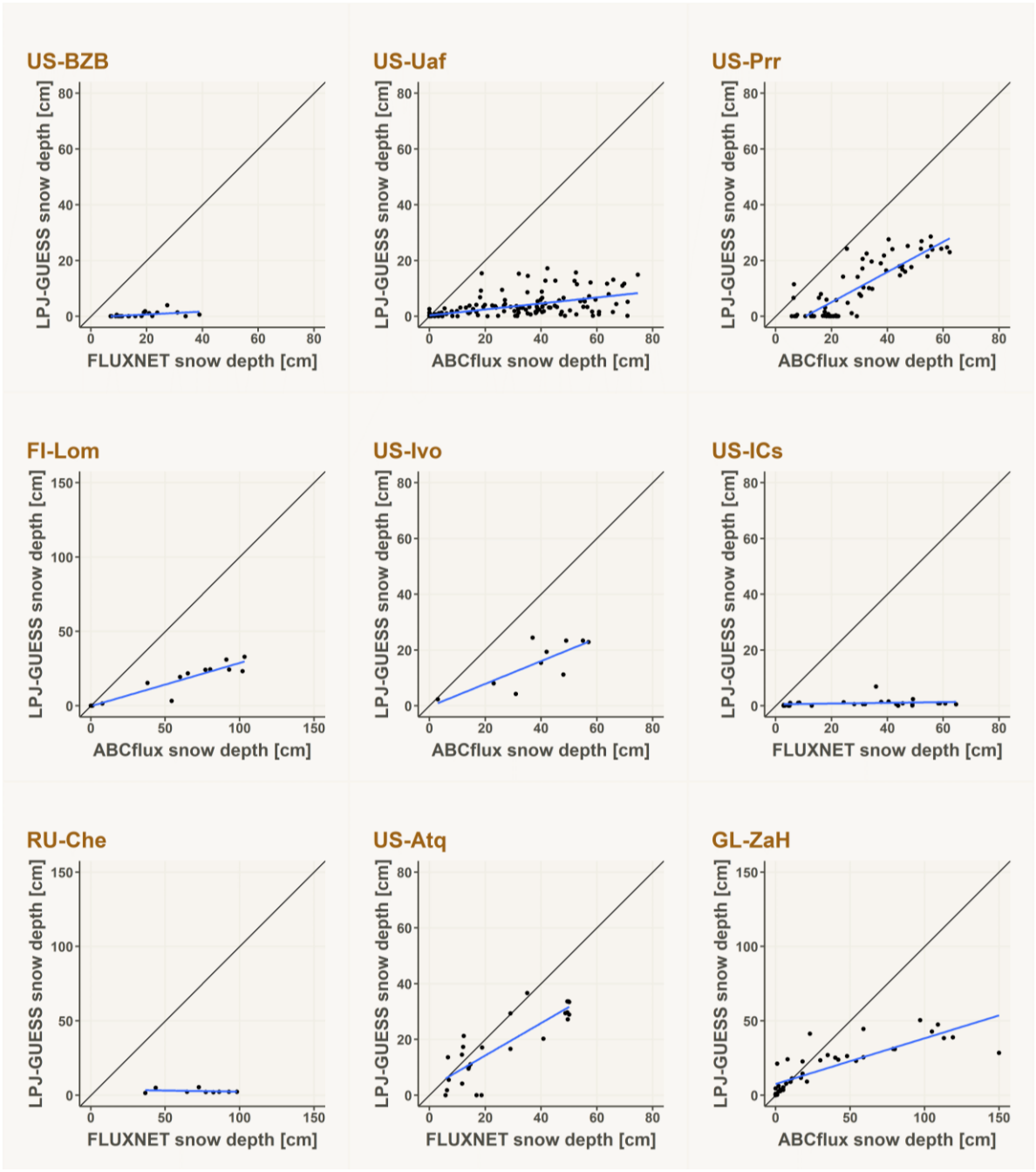

Figure 12. Monthly snow depth. Simulated values are taken from the bias corrected upland run. Observations are from the FLUXNETCH4 dataset for US-Atq, US-BZB, UC-Ics and RU-Che. The observations for the other sites are taken from the ABCflux dataset.

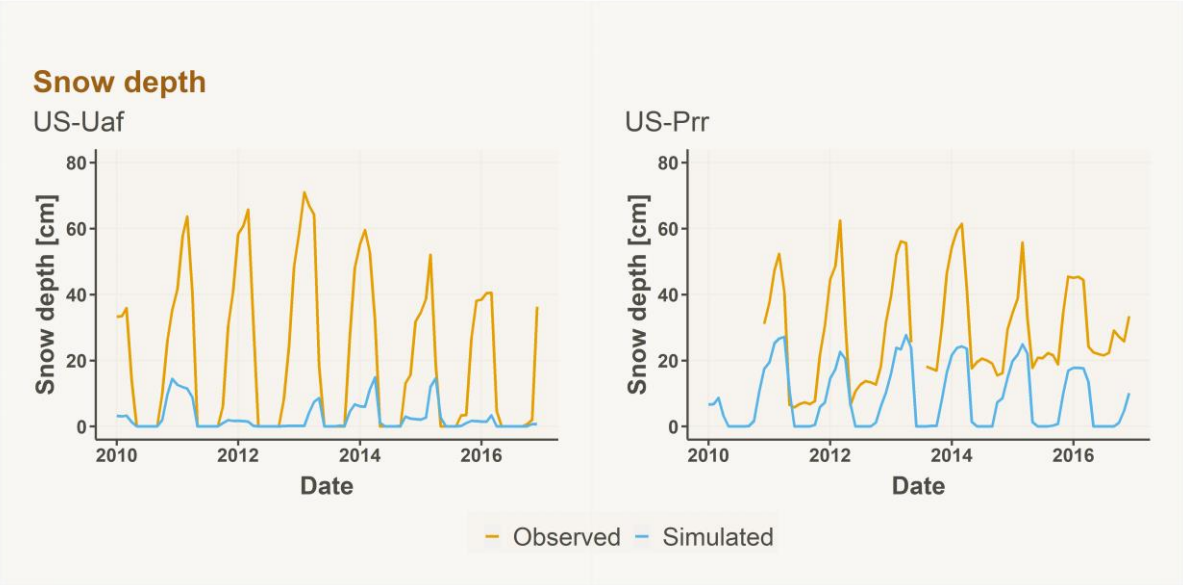

Figure 13. Mean monthly snow depth for the years 2010-2016 for US-Uaf (left) and US-Prr (right). Observations are taken from the ABCflux dataset.

For one site, observations for the snow depth during May were available from the CALM database (see *Figure 14*). The red points show the simulated snow depth when running the model with the bias corrected climate forcing. This plot shows that LPJ-GUESS captured the snow depth during May very well. For almost all years, the simulated value was within one standard deviation from the mean.

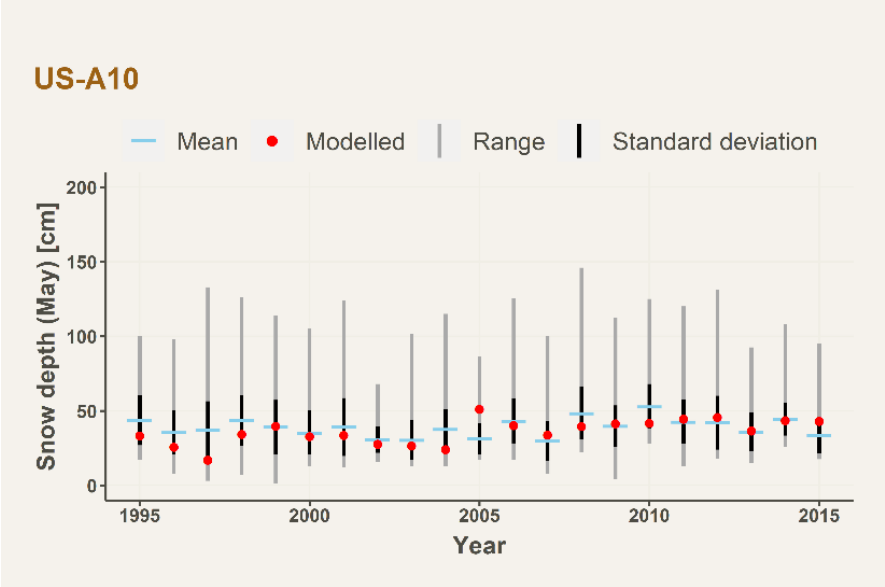

Figure 14. Snow depth during May for US-A10. Mean, range and standard deviation represent the CALM observations. Red points show the simulated output for the upland run.

5 Discussion

5.1 Snow depth

The simulated snow depth was for almost all months lower than the observations from the FLUXNET CH4 and ABCflux datasets. Yet, the CALM observations at US-A10 showed that LPJ-GUESS simulated the snow depth in May accurately.

For some sites, the amount of precipitation during the cold season is likely to be the cause of the low amount of snow simulated by LPJ-GUESS. These Arctic sites have a relatively low mean annual precipitation, commonly between 150 to 300 mm. There are usually large uncertainties in precipitation observations and performing an accurate bias correction is complex. This might have resulted in an incorrect representation of the amount of snow during the winter, which in turn resulted in a too small snowpack.

The reliability of the FLUXNET CH4 and ABCflux observations for snow depth can be questioned. At US-Atq and US-Prr, for example, the daily snow depth never reaches 0 cm. For certain days in the FLUXNET CH4 dataset the snow depth turns negative. It is likely that the gap-filling methodology has not been applied correctly. As there is limited metadata available for these two datasets, it is not known whether the snow depth observations are obtained by single-point measurements or whether they represent a mean of several measurements. As snow depth is largely dependent on microtopography, single-point measurements may not provide a correct representation of the snow depth across the entire site (Chadburn et al. 2017).

A sensitivity analysis could improve our understanding of which parameters influence the simulated snow depth and thus could be used for tuning the model. The multi-layer snow scheme adopted in the Joint UK Land Environment Simulator (JULES), which is a land surface model (LSM), shows certain similarities to the dynamic snow scheme applied in LPJ-GUESS. The same methodology, based on Best et al. (2011), is used to derive the thermal conductivity and the snow density through compaction in both models. Parameters that are known to affect the snow density in JULES could therefore be included in a sensitivity analysis.

A study by Vikhamar-Schuler et al. (2012) has shown that lowering the fresh snow density from 250 kg m^{-3} to 100 kg m^{-3} improved the snow depth simulated by the multi-layer snow scheme of JULES. For LPJ-GUESS the snow depth is calculated dynamically and is dependent on various constants and the wind speed at 10 m above the surface. The minimum snow density is set to 150 kg m^{-3}.

Snow density of each layer increases as a result of compaction calculated as described in Best et al. (2011). Experiments conducted by Kojima (1967) were used to define this approach. In these experiments the fresh snow densities where in the range of 50 to 70 kg m^{-3} and the snow temperatures within

268 to 273 K. These characteristics differ from what is applied in LPJ-GUESS and could affect the simulated snow depth.

A study by Yang et al. (2020) showed that JULES is highly sensitive to the compactive viscosity factor (η_k) used to calculate the snow density.

Certain dynamics which affect snow depth are not captured by LPJ-GUESS. Shrubs are, for example, known to trap snow (Liston et al. 2002) but this process is not included in the model. This affects in turn the soil temperature and thus also ALT.

5.2 Active layer thickness

The end-of-season ALT is largely overestimated by LPJ-GUESS in upland soils. This is also a problem for other DGVMs, such as ORCHIDEE and JSBACH, which simulate too high soil temperatures during the summer months (Chadburn et al. 2017).

The wetness of the active layer is affected by the underlying permafrost. As permafrost is largely impermeable, little water can infiltrate. For this reason, the active layer is often (close to) being fully saturated (Sturm et al. 2005). In LPJ-GUESS, wetlands consist of three acrotelm layers with a varying water table and twelve permanently saturated catotelm layers. Therefore, the true conditions of the active layer may be captured more accurately by the wetlands run.

Running the model with peat soils lowered the ALT. This may be explained by the amount of soil organic matter (SOM). The amount of SOM is higher for peatlands, which affects phase changes and thus lowers the soil temperature. Furthermore, the thermal conductivity of peat is substantially lower ($0.58 \cdot 10^6$ J m^{-3} K^{-1}) than for minerals ($2.38 \cdot 10^6$ J m^{-3} K^{-1}). Peat soils are highly porous due to the high content of SOM, which affects the thermal conductivity as well (Dyukarev et al. 2020). The shallower ALT resulted in a very good fit for the wet forest sites. At wetland sites the reduction in ALT was too high and consequently led to an underestimation.

An additional factor contributing to the contrasting ALT between the wetlands and upland runs can be attributed to the sensitivity of thermal diffusivity to soil water content. The calculation of thermal diffusivity occurs on a monthly basis, utilizing the average soil water content from the preceding month. The relationship between thermal diffusivity and water content is not linear; it demonstrates a rapid incline with increasing water content until it culminates at a water volume fraction of 0.15, followed by a gradual decline (van Duin 1963).

For the upland run, a lower soil water content can be observed, leading to an elevated thermal diffusivity. Consequently, the heightened thermal diffusivity facilitates a swifter release of heat. The accelerated heat release potentially accounts for the higher soil temperatures, with an amplification in ALT as result.

This intricate interplay of thermal diffusivity and water content contributes to the observed disparities in ALT between the wetlands and upland runs.

ALT is greatly influenced by soil properties, such as the ice content (Smith et al. 2010). To further evaluate the reasons behind the incorrect representation of ALT at wetlands additional data on these properties would be necessary. The ALT for US-Uaf (*Figure 11*) is better captured by the wetlands than upland run. The soil temperature behaviour for the wetlands run might initially appear unusual, with the plateau observed at 0 ºC. This consistent temperature of 0 ºC is attributed to the implementation of phase changes in the LPJ-GUESS model. The method for incorporating phase changes follows a straightforward approach as detailed in Wania et al. (2009). Whenever water transitions between its liquid and solid phases or vice versa, the soil temperature is set to 0 ºC. This thermal condition persists until the entirety of the water present has undergone the phase transition.

5.3 Carbon fluxes

For the wet forest sites, it was possible to model the ALT correctly on peat soils. However, as by default no trees are able to grow in these conditions, the GPP was largely reduced. To improve the model's performance by increasing the simulated GPP, two needleleaved evergreen tree PFTs (BNE and BINE) were added. These two new PFTs were not parameterized. To get a better fit, it would be required to further look at the parameters affecting GPP to ensure that the traits of the tree PFTs are properly captured. For instance, the duration of inundation that they can withstand and their specific leaf area (SLA) could be adjusted.

Introducing other tree PFTs could also improve the model's performance. All the wet forest sites included in this study were dominated by evergreen needleleaved tress. For this reason, only BNE and BINE were included in the wetlands with trees simulation. However, at some wetland sites, such as RU-Che, larch trees are highly abundant. Including BNS might therefore improve the model fit for this particular site.

For the sites located furthest up north, roughly exceeding 70ºN, the simulated GPP was close to 0 gC m^{-2} d^{-1}. This can be explained by the low temperatures that limits growth and net photosynthetic rates. The establishment of shrubs and trees in LPJ-GUESS is constrained by a GDD5 threshold, which is not met for these high Arctic sites. Other DGVMs show similar problems with simulating shrubs at high latitude sites caused by this GDD5 establishment constraint (Zhu et al. 2018).

It is relevant to represent mosses correctly in the model for accurately simulating the ecosystem's productivity. This is especially true for wetlands where mosses are widely abundant (Turetsky et al. 2010).

Errors in simulated GPP are propagated to related model output, such as biomass and other carbon fluxes (Schaefer et al. 2012). Parameter tuning of the Arctic PFTs could improve the performance of LPJ-GUESS. Various studies have shown that SLA can greatly affect GPP (Pappas et al. 2013; Renwick et al. 2019; Zheng et al. 2023). In this study SLA was calculated from the PFT's leaf longevity. The leaf longevity of black spruce, the dominant tree species at most forest sites in this study, is 50-60 months (Reich et al. 1998) which can be used to parameterize the corresponding PFT (BNE).

The difference in the observed and simulated R_{eco} was very similar as for GPP. However, in general the slope of the linear fit for R_{eco} was smaller than for GPP which resulted in an underestimation of R_{eco} at most sites. For the wetlands (with trees) run the ALT was too shallow, as compared to the observations, which meant that the soil temperatures were too low. This would in turn have slowed down the rate of decomposition and thus reduced R_{eco}.

5.4 Ancillary variables

More ancillary data would have allowed for a more in-depth model evaluation and analysis of the main limitations of LPJ-GUESS. LAI and GPP are, for example, closely related (Chadburn et al. 2017). It would therefore have been of interest to verify whether LPJ-GUESS can simulate LAI accurately, but US-Uaf was the only site with available observations.

5.4.1 Leaf area index

At US-Uaf the LAI was largely overestimated by LPJ-GUESS for the upland run. The overestimation of LAI by DGVMs is a known problem (Murray-Tortarolo et al. 2013; Renwick et al. 2019). Moreover, LPJ-GUESS failed to capture the seasonal patterns with little variation in the simulated LAI during winter and summer. The large range in LAI for the wetlands with trees run may be due to the abundance of peatland moss. LPJ-GUESS only allows for this PFT to establish during the growing season and contributes substantially to the total LAI during those months.

An incorrect representation of LAI in the model may lead to discrepancies in the vegetation carbon fluxes. An overestimation in LAI, and thus GPP, may sometimes be explained by how gap dynamics and competition are incorporated in the model (Murray-Tortarolo et al. 2013). It can therefore also be an indicator for an incorrect representation of the PFT distribution.

During the winter months, LPJ-GUESS simulates a constant value for LAI. This is due to the presence of evergreen vegetation and the climate not allowing for any growth. Once the amount of incoming solar radiation and the air temperature increase, summergreen shrubs and grasses can emerge. As a consequence, the LAI increases and shows some variation on a daily scale. When the climatic conditions become less favourable, the LAI returns to a constant value based on the evergreen shrubs and trees. The observations show, however, a bigger interannual variation that LPJ-GUESS does not capture which can affect the model's performance for the carbon fluxes as well.

5.4.2 Biomass

Many DGVMs are not able to properly simulate AGB (Crisp et al. 2022). This study has shown that the AGB at wet forest sites is best represented by the wetlands (with trees) run. At the two forest sites (US-Uaf and US-Prr) the GPP was underestimated for the wetlands with trees run. This means that when aiming to improve the model fit for GPP, the increase in productivity should not lead to an increase in AGB. Black spruce is dominant at these two sites, which is known to allocate a large amount of biomass belowground (Noguchi et al. 2012). A parameter that could be tuned is Ltor_MAX as this governs the partition of biomass to the leaves and root system (Pappas et al. 2013). It should be noted, however, that the study by Noguchi et al. (2012) reported considerably higher values for AGB than the ABCflux dataset which implies that the quality of the data may be questioned.

5.5 Data quality and availability

The aim of this study was to evaluate the performance of LPJ-GUESS when applied on high latitude sites. FLUXNET is a well-established network based on properly defined protocols to ensure the quality and consistency of the data. The data is reliable and freely available. Add that it might be slightly less reliable in the cold season due to missing observations and thus more gap-filling being required. As a result, it provides a great opportunity for benchmarking on site level. Nevertheless, there are various limitations related to the evaluation data.

One of the main problems is the limited amount of data and its spatial distribution. The AMERIFLUX sites in the United States are well-represented, whereas none of the sites are located in Canada. Russia, which comprises a large part of the Arctic, is only represented by two sites. It should be noted, however, that there are a few more sites available under the FLUXNET Tier 2 license.

The FLUXNET2015 dataset has several advantages as opposed to the FLUXNETCH4 Community Product. The FLUXNET2015 dataset includes meteorological data from 1989 to 2014, whereas the FLUXNETCH4 dataset extends over a period of 2 to 7 years. Limited meteorological data may affect the bias correction. The data processing pipeline for FLUXNET2015 allows the user to choose between the various different derived carbon fluxes based on the partition method and u* threshold. It also includes quality flags which can be easily used for checking the data quality. The lack of quality flags for the FLUXNETCH4 dataset may have affected the results of this study. Based on the observations US-A10 is, for example, presumably a rather productive site. However, the GDD5 is low and less than 10% of the area at this site is covered by vegetation. This seems to be inconsistent with the relatively high observed GPP.

The ALT data that was available from the CALM database provides valuable information on the end-of-season ALT. CALM data extends over a long period of time and measurements are taken at 20-121 points within a grid at each site. However, it was not possible to evaluate LPJ-GUESS for the other

parts of the season. The ABCflux dataset included monthly thaw depth observations for US-Uaf, which provided information on the site's behaviour with the different soil types.

6 Conclusions

LPJ-GUESS was run and evaluated for 20 FLUXNET sites. Performing a bias correction of the climate forcing based on meteorological FLUXNET data improved the model's performance in terms of GPP and R_{eco} for almost all sites. The model was not able to capture GPP and R_{eco} at high latitude (>70°N) sites as it simulated values close to 0 gC m^{-2} d^{-1} which is not in correspondence with the observations.

Most of the sites that were included in this study were wetlands. For this reason, one of the runs that was evaluated included wetland PFTs and peatland soils. Many wetlands showed an underestimation in both GPP and R_{eco}. ALT at these sites was either too high (upland run) or too low (wetlands run) when comparing it to CALM observations.

To improve the model's representation of wet forests, LPJ-GUESS was run using the same set-up as for the wetlands run, but this time boreal evergreen needleleaved tree PFTs were included as well. This resulted in a good simulation of end-of-season ALT. However, it also implied an underestimation of both GPP and R_{eco}.

Snow depth is poorly modelled at all sites for which there was data available. It should be noted that the quality of some of the observed data can be questioned. Nevertheless, LPJ-GUESS seems to simulate a low snow depth which is unlikely to correspond to the real situation at these high latitude sites.

As climate change continues to exert profound impacts on the Arctic region, there is an escalating urgency to comprehend its consequences. Significant advancements in refining the LPJ-GUESS model have been undertaken to enhance its applicability in the Arctic context. However, despite these efforts, this research underscores the presence of substantial disparities between model projections and actual observations of relevant Arctic parameters.

These divergences may originate from the inherent uncertainties in climate forcing data or stem from inadequacies in the representation of specific processes within the model. Addressing these challenges remains pivotal to refining the model's accuracy. By doing so, we can deepen our comprehension of carbon fluxes within Arctic ecosystems and gain a better perspective on how these ecosystems are likely to evolve in the face of future change.

7 References

Best, M. J., M. Pryor, D. B. Clark, G. G. Rooney, R. L. H. Essery, C. B. Ménard, J. M. Edwards, M. A. Hendry, et al. 2011. The Joint UK Land Environment Simulator (JULES), model description – Part 1: Energy and water fluxes. *Geoscientific Model Development* 4: 677–699. doi:10.5194/gmd-4-677-2011.

Biskaborn, B. K., S. L. Smith, J. Noetzli, H. Matthes, G. Vieira, D. A. Streletskiy, P. Schoeneich, V. E. Romanovsky, et al. 2019. Permafrost is warming at a global scale. *Nature Communications* 10: 264. doi:10.1038/s41467-018-08240-4.

Blume-Werry, G., A. Milbau, L. M. Teuber, M. Johansson, and E. Dorrepaal. 2019. Dwelling in the deep – strongly increased root growth and rooting depth enhance plant interactions with thawing permafrost soil. *New Phytologist* 223: 1328–1339. doi:10.1111/nph.15903.

Box, J. E., W. T. Colgan, T. R. Christensen, N. M. Schmidt, M. Lund, F.-J. W. Parmentier, R. Brown, U. S. Bhatt, et al. 2019. Key indicators of Arctic climate change: 1971–2017. *Environmental Research Letters* 14: 045010. doi:10.1088/1748-9326/aafc1b.

Brown, J., K. M. Hinkel, and F. E. Nelson. 2000. The Circumpolar Active Layer Monitoring (CALM) program: Research designs and initial results. *Polar Geography* 24: 165–258.

Bruhwiler, L., F.-J. W. Parmentier, P. Crill, M. Leonard, and P. I. Palmer. 2021. The Arctic carbon cycle and its response to changing climate. *Current Climate Change Reports* 7: 14–34. doi:10.1007/s40641-020-00169-5.

Burn, C. R. 1998. The active layer: Two contrasting definitions. *Permafrost and Periglacial Processes* 9: 411–416.

Chadburn, S. E., G. Krinner, P. Porada, A. Bartsch, C. Beer, L. Belelli Marchesini, J. Boike, A. Ekici, et al. 2017. Carbon stocks and fluxes in the high latitudes: Using site-level data to evaluate Earth system models. *Biogeosciences* 14: 5143–5169. doi:10.5194/bg-14-5143-2017.

Chicco, D., M. J. Warrens, and G. Jurman. 2021. The coefficient of determination R-squared is more informative than SMAPE, MAE, MAPE, MSE and RMSE in regression analysis evaluation. *PeerJ Computer Science* 7: e623. doi:10.7717/peerj-cs.623.

Chylek, P., C. Folland, J. D. Klett, M. Wang, N. Hengartner, G. Lesins, and M. K. Dubey. 2022. Annual mean Arctic Amplification 1970–2020: Observed and simulated by CMIP6 climate models. *Geophysical Research Letters* 49. doi:10.1029/2022GL099371.

Crisp, D., H. Dolman, T. Tanhua, G. A. McKinley, J. Hauck, A. Bastos, S. Sitch, S. Eggleston, et al. 2022. How well do we understand the land-ocean-atmosphere carbon cycle? *Reviews of Geophysics* 60. doi:10.1029/2021RG000736.

Delwiche, K. B., S. H. Knox, A. Malhotra, E. Fluet-Chouinard, G. McNicol, S. Feron, Z. Ouyang, D. Papale, et al. 2021. FLUXNET-CH4: A global, multi-ecosystem dataset and analysis of methane seasonality from freshwater wetlands. *Earth System Science Data* 13: 3607–3689. doi:10.5194/essd-13-3607-2021.

van Duin, R. H. A. 1963. *The influence of soil management on the temperature wave near the soil surface*. (Technical Bulletin / Institute for Land and Water Management Research; No. 29.

Dyukarev, E. A., A. A. Vyaizya, and K. V. Kiselev. 2020. Differences in temperature regime of mineral and peat soil in Bakchar district of Tomsk region. *Environmental Dynamics and Global Climate Change* 10: 100–109. doi:10.17816/edgcc21323.

Elmendorf, S. C., G. H. R. Henry, R. D. Hollister, R. G. Björk, N. Boulanger-Lapointe, E. J. Cooper, J. H. C. Cornelissen, T. A. Day, et al. 2012. Plot-scale evidence of tundra vegetation change and links to recent summer warming. *Nature Climate Change* 2: 453–457. doi:10.1038/nclimate1465.

Epstein, H. E., M. K. Raynolds, D. A. Walker, U. S. Bhatt, C. J. Tucker, and J. E. Pinzon. 2012. Dynamics of aboveground phytomass of the circumpolar Arctic tundra during the past three decades. *Environmental Research Letters* 7: 015506. doi:10.1088/1748-9326/7/1/015506.

Eugster, W., W. R. Rouse, R. A. Pielke Sr, J. P. Mcfadden, D. D. Baldocchi, T. G. F. Kittel, F. S. Chapin, G. E. Liston, et al. 2000. Land–atmosphere energy exchange in Arctic tundra and boreal forest: Available data and feedbacks to climate. *Global Change Biology* 6: 84–115. doi:10.1046/j.1365-2486.2000.06015.x.

Farquhar, G. D., and S. von Caemmerer. 1982. Modelling of Photosynthetic Response to Environmental Conditions. In *Physiological Plant Ecology II*, ed. O. L. Lange, P. S. Nobel, C. B. Osmond, and H. Ziegler, 549–587. Berlin, Heidelberg: Springer Berlin Heidelberg. doi:10.1007/978-3-642-68150-9_17.

Gruber, S. 2012. Derivation and analysis of a high-resolution estimate of global permafrost zonation. *The Cryosphere* 6: 221–233. doi:10.5194/tc-6-221-2012.

Gustafson, A., P. A. Miller, R. G. Björk, S. Olin, and B. Smith. 2021. Nitrogen restricts future sub-arctic treeline advance in an individual-based dynamic vegetation model. *Biogeosciences* 18: 6329–6347. doi:10.5194/bg-18-6329-2021.

Harris, S. A., H. M. French, J. A. Heignbottom, G. H. Johnston, B. Ladanyi, D. C. Sego, and R. O. van Everdingen, ed. 1988. *Glossary of permafrost and related ground-ice terms*. Technical Memorandum / National Research Council, Canada 142. Ottawa,Ontario,Canada.

Jonasson, S., and G. R. Shaver. 1999. Within-stand nutrient cycling in Arctic and boreal wetlands. *Ecology* 80: 2139–2150. doi:10.1890/0012-9658(1999)080[2139:WSNCIA]2.0.CO;2.

Jones, H. 2013. Energy balance and evaporation. In *Plants and microclimate: A quantitative approach to environmental plant physiology*, 99–121. Cambridge: Cambridge University Press.

Kåresdotter, E., G. Destouni, N. Ghajarnia, G. Hugelius, and Z. Kalantari. 2021. Mapping the vulnerability of Arctic wetlands to global warming. *Earth's Future* 9. doi:10.1029/2020EF001858.

Kasurinen, V., K. Alfredsen, P. Kolari, I. Mammarella, P. Alekseychik, J. Rinne, T. Vesala, P. Bernier, et al. 2014. Latent heat exchange in the boreal and arctic biomes. *Global Change Biology* 20: 3439–3456. doi:10.1111/gcb.12640.

Kira, O., C. Y-Y. Chang, L. Gu, J. Wen, Z. Hong, and Y. Sun. 2021. Partitioning net ecosystem exchange (NEE) of CO2 using solar-induced chlorophyll fluorescence (SIF). *Geophysical Research Letters* 48. doi:10.1029/2020GL091247.

Kojima, K. 1967. Densification of seasonal snow cover. *Physics of Snow and Ice: Proceedings* 1: 929–952.

Lange, S. 2019. Trend-preserving bias adjustment and statistical downscaling with ISIMIP3BASD (v1.0). *Geoscientific Model Development* 12: 3055–3070. doi:10.5194/gmd-12-3055-2019.

Lange, S. 2022. ISIMIP3BASD (version 3.0.2). Zenodo. doi:10.5281/ZENODO.7151476.

Lasslop, G., M. Reichstein, D. Papale, A. D. Richardson, A. Arneth, A. Barr, P. Stoy, and G. Wohlfahrt. 2010. Separation of net ecosystem exchange into assimilation and respiration using a light response curve approach: critical issues and global evaluation. *Global Change Biology* 16: 187–208. doi:10.1111/j.1365-2486.2009.02041.x.

Liston, G. E., J. P. Mcfadden, M. Sturm, and R. A. Pielke. 2002. Modelled changes in arctic tundra snow, energy and moisture fluxes due to increased shrubs: *Global Change Biology* 8: 17–32. doi:10.1046/j.1354-1013.2001.00416.x.

Luo, D., Q. Wu, H. Jin, S. S. Marchenko, L. Lü, and S. Gao. 2016. Recent changes in the active layer thickness across the northern hemisphere. *Environmental Earth Sciences* 75: 555. doi:10.1007/s12665-015-5229-2.

Ma, D., X. Wu, X. Ma, J. Wang, X. Lin, and C. Mu. 2021. Spatial, phenological, and inter-annual variations of gross primary productivity in the Arctic from 2001 to 2019. *Remote Sensing* 13: 2875. doi:10.3390/rs13152875.

Martin, A. C., E. S. Jeffers, G. Petrokofsky, I. Myers-Smith, and M. Macias-Fauria. 2017. Shrub growth and expansion in the Arctic tundra: An assessment of controlling factors using an evidence-based approach. *Environmental Research Letters* 12: 085007. doi:10.1088/1748-9326/aa7989.

Meredith, M., M. Sommerkorn, S. Cassotta, C. Derksen, A. Ekaykin, A. Hallowed, G. Kofinas, A. Mackintosh, et al. 2019. Polar regions. In *IPCC special report on the ocean and cryosphere in a changing climate*, ed. H.-O. Pörtner, D. C. Roberts, V. Masson-Delmotte, P. Zhai, M. Tignor, E. Poloczanska, K. Mintenbeck, A. Alegría, et al., 1st ed., 203–320. Cambridge, UK and New York, NY, USA: Cambridge University Press. doi:10.1017/9781009157964.

Miller, P. A., and B. Smith. 2012. Modelling tundra vegetation response to recent Arctic warming. *AMBIO* 41: 281–291. doi:10.1007/s13280-012-0306-1.

Mod, H. K., and M. Luoto. 2016. Arctic shrubification mediates the impacts of warming climate on changes to tundra vegetation. *Environmental Research Letters* 11: 124028. doi:10.1088/1748-9326/11/12/124028.

Murray-Tortarolo, G., A. Anav, P. Friedlingstein, S. Sitch, S. Piao, Z. Zhu, B. Poulter, S. Zaehle, et al. 2013. Evaluation of land surface models in reproducing satellite-derived LAI over the High-latitude Northern Hemisphere. Part I: uncoupled DGVMs. *Remote Sensing* 5: 4819–4838. doi:10.3390/rs5104819.

Myers-Smith, I. H., and D. S. Hik. 2018. Climate warming as a driver of tundra shrubline advance. Edited by Rien Aerts. *Journal of Ecology* 106: 547–560. doi:10.1111/1365-2745.12817.

Noguchi, K., M. Dannoura, M. Jomura, M. Awazuhara-Noguchi, and Y. Matsuura. 2012. High below-ground biomass allocation in an upland black spruce (Picea mariana) stand in interior Alaska. *Polar Science* 6: 133–141. doi:10.1016/j.polar.2011.12.002.

Pappas, C., S. Fatichi, S. Leuzinger, A. Wolf, and P. Burlando. 2013. Sensitivity analysis of a process-based ecosystem model: Pinpointing parameterization and structural issues: *Journal of Geophysical Research: Biogeosciences* 118: 505–528. doi:10.1002/jgrg.20035.

Pastorello, G., C. Trotta, E. Canfora, H. Chu, D. Christianson, Y.-W. Cheah, C. Poindexter, J. Chen, et al. 2020. The FLUXNET2015 dataset and the ONEFlux processing pipeline for eddy covariance data. *Scientific Data* 7: 225. doi:10.1038/s41597-020-0534-3.

Piao, S., P. Ciais, P. Friedlingstein, P. Peylin, M. Reichstein, S. Luyssaert, H. Margolis, J. Fang, et al. 2008. Net carbon dioxide losses of northern ecosystems in response to autumn warming. *Nature* 451: 49–52. doi:10.1038/nature06444.

Pongracz, A. 2019. Snow insulation effects across the Arctic - Evaluating a revised snow module in LPJ-GUESS. MSc thesis, Lund: Lund University.

Pongracz, A., D. Wårlind, P. A. Miller, and F.-J. W. Parmentier. 2021. Model simulations of Arctic biogeochemistry and permafrost extent are highly sensitive to the implemented snow scheme in LPJ-GUESS. *Biogeosciences*. doi:10.5194/bg-2021-121.

Reich, P. B., M. G. Tjoelker, M. B. Walters, D. W. Vanderklein, and C. Buschena. 1998. Close association of RGR, leaf and root morphology, seed mass and shade tolerance in seedlings of nine boreal tree species grown in high and low light: RGR and tissue morphology in boreal trees. *Functional Ecology* 12: 327–338. doi:10.1046/j.1365-2435.1998.00208.x.

Reichle, D. E. 2020. Energy flow in ecosystems. In *The Global Carbon Cycle and Climate Change*, 119–156. Elsevier. doi:10.1016/B978-0-12-820244-9.00008-1.

Reichstein, M., E. Falge, D. Baldocchi, D. Papale, M. Aubinet, P. Berbigier, C. Bernhofer, N. Buchmann, et al. 2005. On the separation of net ecosystem exchange into assimilation and ecosystem respiration: review and improved algorithm. *Global Change Biology* 11: 1424–1439. doi:10.1111/j.1365-2486.2005.001002.x.

Renwick, K. M., A. Fellows, G. N. Flerchinger, K. A. Lohse, P. E. Clark, W. K. Smith, K. Emmett, and B. Poulter. 2019. Modeling phenological controls on carbon dynamics in dryland sagebrush ecosystems. *Agricultural and Forest Meteorology* 274: 85–94. doi:10.1016/j.agrformet.2019.04.003.

Schaefer, K., C. R. Schwalm, C. Williams, M. A. Arain, A. Barr, J. M. Chen, K. J. Davis, D. Dimitrov, et al. 2012. A model-data comparison of gross primary productivity: Results from the North American Carbon Program site synthesis. *Journal of Geophysical Research: Biogeosciences* 117: n/a-n/a. doi:10.1029/2012JG001960.

Schaefer, K., H. Lantuit, V. E. Romanovsky, E. A. G. Schuur, and R. Witt. 2014. The impact of the permafrost carbon feedback on global climate. *Environmental Research Letters* 9: 085003. doi:10.1088/1748-9326/9/8/085003.

Schuur, E. A. G., J. Bockheim, J. G. Canadell, E. Euskirchen, C. B. Field, S. V. Goryachkin, S. Hagemann, P. Kuhry, et al. 2008. Vulnerability of permafrost carbon to climate change: Implications for the global carbon cycle. *BioScience* 58: 701–714. doi:10.1641/B580807.

Schuur, E. A. G., A. D. McGuire, C. Schädel, G. Grosse, J. W. Harden, D. J. Hayes, G. Hugelius, C. D. Koven, et al. 2015. Climate change and the permafrost carbon feedback. *Nature* 520: 171–179. doi:10.1038/nature14338.

Smith, B., D. Wårlind, A. Arneth, T. Hickler, P. Leadley, J. Siltberg, and S. Zaehle. 2014. Implications of incorporating N cycling and N limitations on primary production in an individual-based dynamic vegetation model. *Biogeosciences* 11: 2027–2054. doi:10.5194/bg-11-2027-2014.

Smith, S. L., V. E. Romanovsky, A. G. Lewkowicz, C. R. Burn, M. Allard, G. D. Clow, K. Yoshikawa, and J. Throop. 2010. Thermal state of permafrost in North America: A contribution to the

international polar year. *Permafrost and Periglacial Processes* 21: 117–135. doi:10.1002/ppp.690.

Sturm, M., J. Schimel, G. Michaelson, J. M. Welker, S. F. Oberbauer, G. E. Liston, J. Fahnestock, and V. E. Romanovsky. 2005. Winter biological processes could help convert Arctic tundra to shrubland. *BioScience* 55: 17. doi:10.1641/0006-3568(2005)055[0017:WBPCHC]2.0.CO;2.

Tans, P. 2023. Trends in atmospheric carbon dioxide. NOAA/GML.

Turetsky, M. R., M. C. Mack, T. N. Hollingsworth, and J. W. Harden. 2010. The role of mosses in ecosystem succession and function in Alaska's boreal forest. *Canadian Journal of Forest Research* 40: 1237–1264. doi:10.1139/X10-072.

Ueyama, M. 2018. *US-Uaf site photograph*. Photograph.

Ueyama, M., H. Iwata, and Y. Harazono. 2014. Autumn warming reduces the CO2 sink of a black spruce forest in interior Alaska based on a nine-year eddy covariance measurement. *Global Change Biology* 20: 1161–1173. doi:10.1111/gcb.12434.

University of East Anglia Climatic Research Unit, and I. C. Harris. 2020. CRU JRA v2.1: A forcings dataset of gridded land surface blend of Climatic Research Unit (CRU) and Japanese reanalysis (JRA) data; Jan.1901 - Dec.2019. Centre for Environmental Data Analysis.

University of East Anglia Climatic Research Unit, and I. C. Harris. 2022. CRU JRA v2.3: A forcings dataset of gridded land surface blend of Climatic Research Unit (CRU) and Japanese reanalysis (JRA) data; Jan.1901 - Dec.2021. NERC EDS Centre for Environmental Data Analysis.

Vikhamar-Schuler, D., J. M. Edwards, G. Rooney, and J. Kristiansen. 2012. Evaluation of JULES multilayer snow scheme for Norwegian snow conditions. In *Geophysical Research Abstracts*, EGU2012–EGU3725.

Viovy, N. 2018. CRUNCEP Version 7 - Atmospheric forcing data for the community land model. NetCDF. UCAR/NCAR - Research Data Archive. doi:10.5065/PZ8F-F017.

Virkkala, A.-M., S. Natali, B. M. Rogers, J. D. Watts, K. Savage, S. J. Connon, M. E. Mauritz-tozer, E. A. G. Schuur, et al. 2021. The ABCflux database: Arctic-boreal CO2 Flux and site environmental data, 1989-2020. doi:10.3334/ORNLDAAC/1934.

Virkkala, A.-M., S. M. Natali, B. M. Rogers, J. D. Watts, K. Savage, S. J. Connon, M. Mauritz, E. A. G. Schuur, et al. 2022. The ABCflux database: Arctic–boreal CO2 flux observations and ancillary information aggregated to monthly time steps across terrestrial ecosystems. *Earth System Science Data* 14: 179–208. doi:10.5194/essd-14-179-2022.

Walker, D. A., M. K. Raynolds, F. J. A. Daniëls, E. Einarsson, A. Elvebakk, W. A. Gould, A. E. Katenin, S. S. Kholod, et al. 2005. The Circumpolar Arctic vegetation map. *Journal of Vegetation Science* 16: 267–282.

Wania, R., I. Ross, and I. C. Prentice. 2009. Integrating peatlands and permafrost into a dynamic global vegetation model: 1. Evaluation and sensitivity of physical land surface processes. *Global Biogeochemical Cycles* 23. doi:10.1029/2008GB003412.

Wookey, P. A., R. Aerts, R. D. Bardgett, F. Baptist, K. A. Bråthen, J. H. C. Cornelissen, L. Gough, I. P. Hartley, et al. 2009. Ecosystem feedbacks and cascade processes: understanding their role in the responses of Arctic and alpine ecosystems to environmental change. *Global Change Biology* 15: 1153–1172. doi:10.1111/j.1365-2486.2008.01801.x.

Wutzler, T., A. Lucas-Moffat, M. Migliavacca, J. Knauer, K. Sickel, L. Šigut, O. Menzer, and M. Reichstein. 2018. Basic and extensible post-processing of eddy covariance flux data with REddyProc. *Biogeosciences* 15: 5015–5030. doi:10.5194/bg-15-5015-2018.

Yang, Y., M. Uddstrom, R. Turner, and M. Revell. 2020. Major factors affecting the snow simulations by the JULES in New Zealand. *Meteorological Applications* 27. doi:10.1002/met.1837.

Zhang, W., P. A. Miller, B. Smith, R. Wania, T. Koenigk, and R. Döscher. 2013. Tundra shrubification and tree-line advance amplify arctic climate warming: Results from an individual-based dynamic vegetation model. *Environmental Research Letters* 8: 034023. doi:10.1088/1748-9326/8/3/034023.

Zheng, Y., L. Zhang, P. Li, X. Ren, H. He, Y. Lv, and Y. Ma. 2023. Evaluation of the community land model-simulated specific leaf area with observations over China: Impacts on modeled gross primary productivity. *Forests* 14: 164. doi:10.3390/f14010164.

Zhu, J., X. Zeng, M. Zhang, Y. Dai, D. Ji, F. Li, Q. Zhang, H. Zhang, et al. 2018. Evaluation of the new Dynamic Global Vegetation Model in CAS-ESM. *Advances in Atmospheric Sciences* 35: 659–670. doi:10.1007/s00376-017-7154-7.

Appendix A: Relative humidity conversion

One of the drivers of LPJ-GUESS is relative humidity. However, for some of the FLUXNET sites only data on vapour pressure deficit was available. The CRUJRA dataset provided specific humidity rather than relative humidity. These quantities were therefore converted to relative humidity by applying the equations given below.

Vapour pressure deficit to relative humidity

First the saturated vapour pressure in *Pa* is calculated according to

$$e_{s(T)} = f \cdot \left(611.21 \cdot \exp\left(b \cdot \frac{T}{257.14 + T}\right)\right) \quad \text{(A1)}$$

where T is the air temperature in *°C*, b is an empirical coefficient given by

$$b = 18.678 - (T \,/\, 234.5) \quad \text{(A2)}$$

and f is an empirical coefficient given by

$$f \cong 1.0007 + 3.46 \cdot 10^{-8} \cdot P \quad \text{(A3)}$$

where P is the atmospheric pressure in *Pa*.

Next, the water vapour pressure (e in *Pa*) is derived from the vapour pressure deficit (*VPD* in *Pa*)

$$e = e_{s(T)} - VPD \quad \text{(A4)}$$

Relative humidity (rh) can then be calculated according to

$$rh = e/e_{s(T)} \quad \text{(A5)}$$

Specific humidity to relative humidity

The water vapour pressure (e in *Pa*) is derived from the specific humidity (q)

$$e = \frac{q \cdot P}{0.378 \cdot q + 0.622} \quad \text{(A6)}$$

Relative humidity can then be calculated by using the equations *A1*, *A5* and *A6*.

Appendix B: List of sites

Table B1. FLUXNET2015 sites with the number of observations included in this study for each variable.

Site ID	Site name	Longitude	Latitude	IGBP	GPP	R_{eco}	Meteo
GL-NuF	Nuuk Fen	-51.386	64.131	WET	696	782	9496
US-Prr	Poker Flat Research Range Black Spruce Forest	-147.488	65.124	ENF	459	590	9496
FI-Sod	Sodankyla	26.639	67.362	ENF	1938	3189	9496
RU-Cok	Chokurdakh	147.494	70.829	OSH	696	579	9496
GL-ZaH	Zackenberg Heath	-20.550	74.473	GRA	769	1024	9496
GL-ZaF	Zackenberg Fen	-20.555	74.481	WET	185	193	9496
SJ-Adv	Adventdalen	15.293	78.186	WET	52	140	9496

Table B2. FLUXNET CH4 Community Product sites with the number of observations included in this study for each variable.

Site ID	Site name	Longitude	Latitude	IGBP	Snow	GPP	R_{eco}	Meteo
SE-Deg	Degerö	19.557	64.182	GRA	-	1826	1826	1826
US-BZB	Bonanza Creek Thermokarst Bog	-148.321	64.696	WET	1096	1096	1096	1096
US-BZS	Bonanza Creek Black Spruce	-148.324	64.696	ENF	647	731	731	731
US-NGC	NGEE Arctic Council	-163.700	64.862	GRA	-	221	457	457
US-Uaf	University of Alaska, Fairbanks	-147.856	64.866	ENF	-	2860	2922	2922
Fi-Lom	Lompolojankka	24.209	67.997	WET	-	1826	1826	1826
US-Ivo	Ivotuk	-155.750	68.487	WET	-	1235	1461	1461
US-ICs	Imnavait Creek Watershed Wet Sedge	-149.311	68.606	WET	1095	1095	1095	1095
RU-Che	Cherski	161.341	68.613	WET	599	980	1083	1096
US-Atq	Atqasuk	-157.409	70.470	WET	817	783	1100	1100
US-NGB	NGEE Arctic Barrow	-156.609	71.280	SNO	-	1112	2554	2557
US-Bes	Barrow-Bes	-156.597	71.281	WET	-	796	1095	1095
US-A10	ARM-NSA-Barrow	-155.615	71.324	BSV	-	2215	2540	2557

Table B3. CALM sites used in this study with the number of data points per grid and the temporal extent.

Site ID	Site code	Site name	Longitude	Latitude	Nr. Points
US-BZS	U18	Bonanza Creek	-148.133	64.7	20
US-Ivo	U26	Ivotuk 1km Grid	-155.733	68.483	121
US-ICs	U11B	Imnavait Creek Wet	-149.315	68.611	71
US-Atq	U3	Atqasuk	-157.400	70.450	121
US-A10	U1	Barrow	-156.6	71.317	121
GL-ZaH	G1	Zackenberg ZEROCALM 1	-20.553	74.473	121

Appendix C: Gross primary productivity

Table C1. RMSE and R^2 for GPP for each site and run, where BC stands for "bias corrected". For each site, the RMSE belonging to a certain simulation is indicated by an asterisk (*), which depends on the type of ecosystem. The BC wetlands run is marked for wetlands and grasslands. The BC wetlands with trees run is marked for wet forests. Other sites (e.g. dominated by shrubs, or forests on dry soils) are represented by the BC upland run. The table is sorted on latitude, where SJ-Adv is furthest north.

	RMSE (gC m^{-2} d^{-1})				R^2			
Site	**CRUJRA upland**	**BC upland**	**BC wetlands**	**BC wetlands with trees**	**CRUJRA upland**	**BC upland**	**BC wetlands**	**BC wetlands with trees**
GL-NuF	2.18	1.27	1.39*	1.40	0.13	0.37	0.21	0.21
SE-Deg	5.70	4.81	2.86*	5.40	0.74	0.68	0.70	0.66
US-BZB	2.63	2.17	1.60*	1.51	0.73	0.72	0.68	0.68
US-BZS	1.83	1.70	1.95	1.96*	0.83	0.83	0.81	0.77
US-NGC	2.60	5.01	1.58*	1.91	0.81	0.86	0.82	0.77
US-Uaf	4.20	3.96	4.89	4.16*	0.17	0.19	0.06	0.19
US-Prr	3.72	3.37	1.91	1.01*	0.59	0.44	0.32	0.46
FI-Sod	2.58	1.26*	1.43	1.41	0.66	0.67	0.55	0.65
FI-Lom	5.48	3.37	1.78*	2.51	0.44	0.47	0.45	0.11
US-Ivo	2.22	1.60	1.87*	1.87	0.72	0.78	0.75	0.75
US-ICs	1.87	0.88	1.56*	1.56	0.66	0.78	0.65	0.65
RU-Che	1.70	1.34	2.37*	2.37	0.75	0.57	0.51	0.51
US-Atq	1.15	1.03	0.96*	0.96	0.79	0.85	0.80	0.80
RU-Cok	2.25	3.59*	3.68	3.68	0.59	0.49	0.26	0.26
US-NGB	1.67	1.68*	1.68	1.68	0.37	0.24	0.50	0.50
US-Bes	2.85	2.85	2.85*	2.85	0.00	0.00	0.00	0.00
US-A10	3.71	3.65*	3.60	3.62	0.05	0.08	0.08	0.09
GL-ZaH	1.34	1.31	1.05*	1.05	0.01	0.34	0.41	0.41
GL-ZaF	4.30	4.27	4.07*	4.07	0.01	0.68	0.88	0.88
SJ-Adv	1.11	1.11	1.12*	1.12	0.99	0.94	0.67	0.67

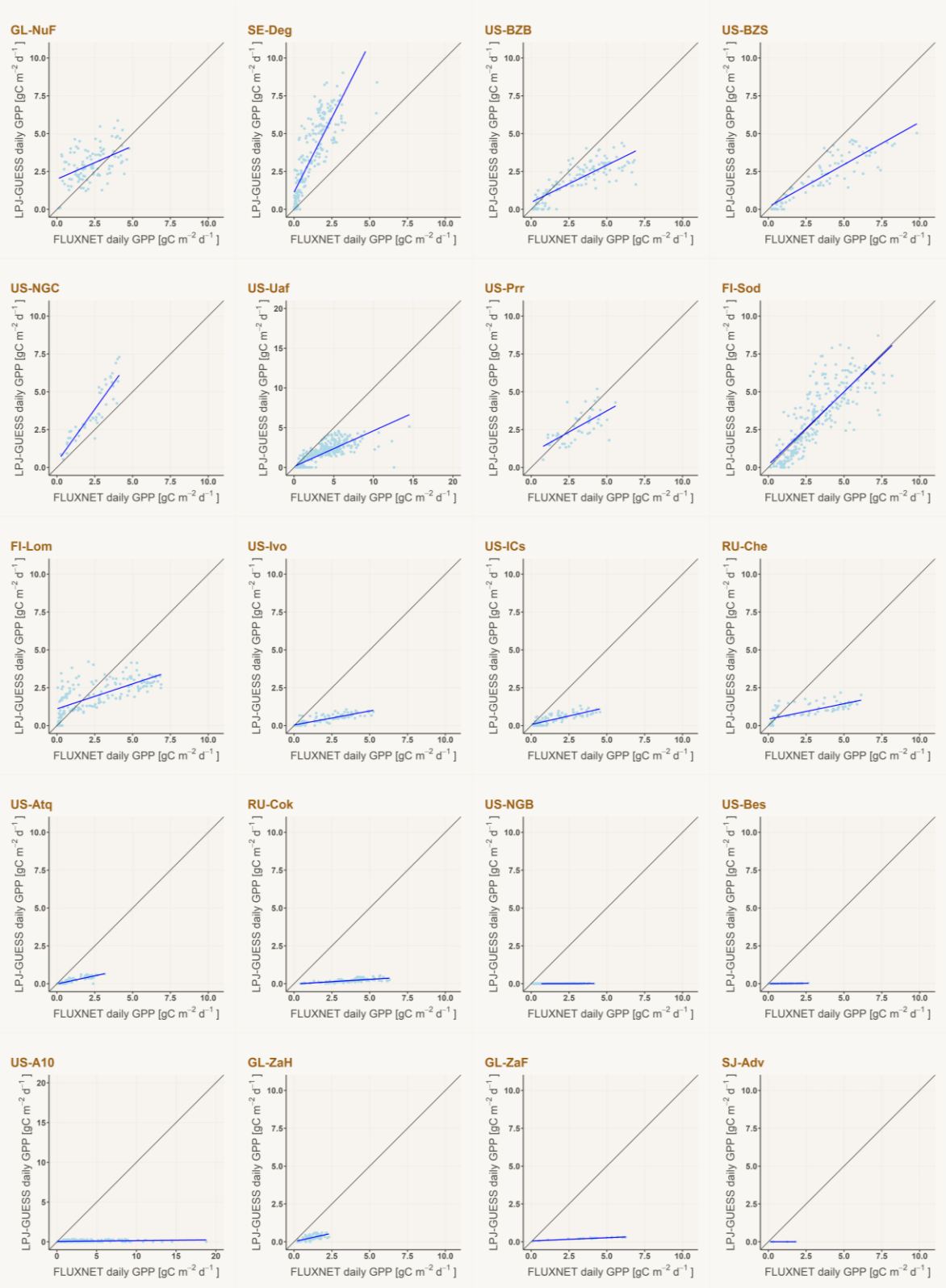

Figure C1. Daily GPP taken as a mean over a period of five days. The simulated values are taken from the run marked with an asterisk in Table C1. The plots are sorted on latitude, where SJ-Adv is furthest north.

Appendix D: Ecosystem respiration

Table D1. RMSE and R^2 for R_{eco} for each site and run, where BC stands for "bias corrected". For each site, the RMSE belonging to a certain simulation is indicated by an asterisk (*), which depends on the type of ecosystem. The BC wetlands run is marked for wetlands and grasslands. The BC wetlands with trees run is marked for wet forests. Other sites (e.g. dominated by shrubs, or forests on dry soils) are represented by the BC upland run. The table is sorted on latitude, where SJ-Adv is furthest north.

	RMSE (gC m^{-2} d^{-1})				R^2			
Site	**CRUJRA upland**	**BC upland**	**BC wetlands**	**BC wetlands with trees**	**CRUJRA upland**	**BC upland**	**BC wetlands**	**BC wetlands with trees**
GL-NuF	1.53	0.58	0.56*	0.56	0.29	0.54	0.50	0.50
SE-Deg	3.23	3.02	1.29*	2.35	0.81	0.82	0.80	0.80
US-BZB	1.75	1.51	1.28*	1.31	0.76	0.74	0.69	0.65
US-BZS	1.14	1.09	2.26	2.28*	0.85	0.85	0.82	0.77
US-NGC	1.61	3.29	0.55*	0.71	0.73	0.76	0.84	0.82
US-Uaf	3.37	3.28	3.82	3.59*	0.21	0.20	0.14	0.21
US-Prr	2.91	2.66	0.95	0.70*	0.80	0.76	0.71	0.7
FI-Sod	1.33	0.80*	1.58	1.67	0.84	0.87	0.81	0.82
FI-Lom	2.44	1.28	0.76*	0.93	0.93	0.88	0.87	0.40
US-Ivo	1.07	0.78	0.94*	0.94	0.79	0.74	0.77	0.77
US-ICs	1.15	0.82	1.06*	1.06	0.56	0.58	0.57	0.57
RU-Che	0.54	0.75	0.99*	0.99	0.84	0.87	0.80	0.80
US-Atq	0.61	0.55	0.52*	0.52	0.64	0.66	0.67	0.67
RU-Cok	1.08	2.01*	2.04	2.04	0.67	0.70	0.39	0.39
US-NGB	0.65	0.65*	0.65	0.65	0.23	0.16	0.29	0.29
US-Bes	2.67	2.67	2.67*	2.67	0.01	0.01	0.01	0.01
US-A10	2.39	2.37*	2.35	2.35	0.01	0.03	0.02	0.02
GL-ZaH	0.80	0.78	0.67*	0.67	0.10	0.38	0.39	0.39
GL-ZaF	1.25	1.24	1.19*	1.19	0.88	0.89	0.82	0.82
SJ-Adv	0.56	0.55	0.56*	0.56	0.81	0.78	0.41	0.41

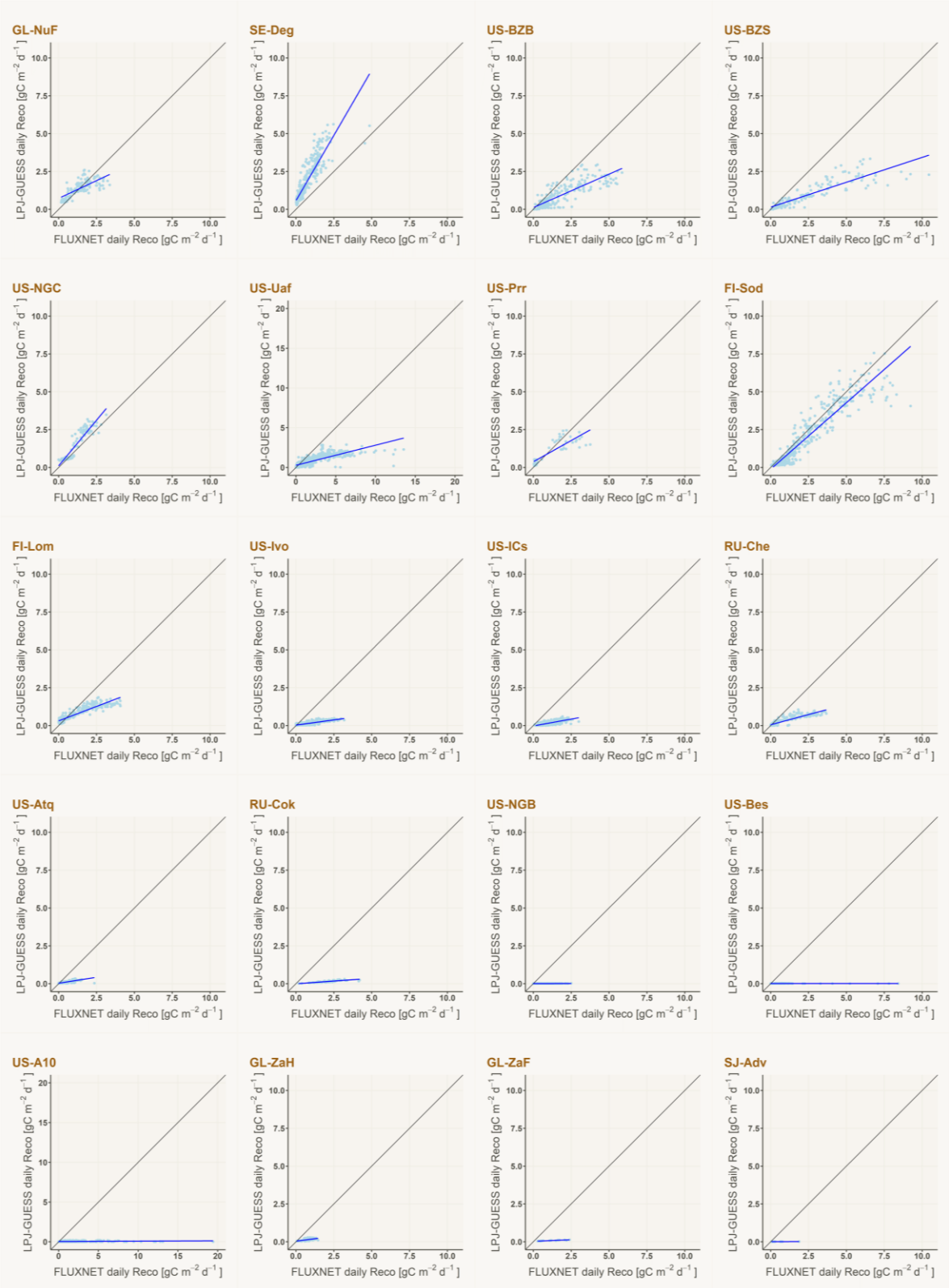

Figure D1. Daily R_{eco} taken as a mean over a period of five days. The simulated values are taken from the run marked with an asterisk in Table D1. The plots are sorted on latitude, where SJ-Adv is furthest north.